SPHERICAL PRESSURE PROBE FOR RETRIEVING FREESTREAM PRESSURE AND DIRECTIONAL DATA

by

William A. Figueiredo

GT&PDL Report No. 137 August 1977

GAS TURBINE & PLASMA DYNAMICS LABORATORY
MASSACHUSETTS INSTITUTE OF TECHNOLOGY
CAMBRIDGE, MASSACHUSETTS

SPHERICAL PRESSURE PROBE FOR RETRIEVING FREESTREAM PRESSURE AND DIRECTIONAL DATA

by

William A. Figueiredo

GT&PDL Report No. 137 August 1977

This research was carried out in the Gas Turbine & Plasma Dynamics Laboratory, M.I.T., supported by the NASA Lewis Research Center under Grant NGL 22-009-383.

ABSTRACT

A spherical pressure probe designed to time resolve the total and static pressure and freestream radial and rotational flow angles in turbomachine flow fields was found to produce accurate results for flow angles over a range of ± 20° in both the radial and rotational directions. Reynolds number based on the probe sphere diameter had negligible effect over the range 14,000 to 92,000. There is a weak Mach number dependence, but the probe is usable up to a Mach number of 0.90. Calibration curves are plotted for M = 0.27, 0.7, and 0.9. These results were found by calibration in steady flow. From the probe dimensions and transducer response it is judged that the probe should have frequency response better than 30 kHz.

I. INTRODUCTION - PROBE DESIGN DEVELOPMENT

Design Purpose

The spherical probe was developed for use in the MIT Blowdown Compressor Facility. In this facility compressor rotors are tested in a pulsed or "blowdown" mode. The pressure probe traverses the compressor annulus during the (20 ms) blowdown to retrieve a time resolved record of local static and total pressure and local rotational and radial flow directions. The data is recorded as a function of time, and hence of radial position at selected axial positions. The mean Mach number in the annulus is approximately 0.7 and the Reynolds number (based on probe diameter) is around 26,000. The probe calibration is focussed on these Mach number and Reynolds number requirements.

The probe must resolve pressure data between compressor blades at blade passing frequency (about 3 KHz). From past probe development experience with this facility, a frequency response of 30 to 60 KHz is needed and can be obtained with a properly designed pressure probe.

Design Configuration

A probe configuration meeting the design specifications took the form of a spherical probe body with 5 strategically placed pressure transducers (Fig. 2). This spherical probe has 5 flat faces with machined seats for attaching high frequency response pressure transducers (Fig. 3). The probe sphere is set on a stem emanating from the probe body carrying transducer connections. This stem is located near the P_5 pressure transducer because of manufacturing constraints and does not introduce serious stem effects.

Data Recovery

This probe was required to retrieve directional data in two planes, θ and ϕ (labeled in Fig. 4), where the θ-plane is perpendicular to the probe stem and the ϕ-plane is parallel to the stem. To retrieve accurate directional data, 3 pressure transducers should be positioned in the desired directional plane to maximize directional sensitivity (P_2, P_1, and P_3 for the θ-plane, P_4, P_1, and P_5 for the ϕ-plane). For example, P_2 and P_3 measure θ-directional components of the freestream while P_1 is required to measure a correctional pressure for ϕ-components of the freestream. With proper calibration function of P_1, P_2, and P_3, ϕ-components of the freestream direction can be normalized out of θ-directional data. The calibration function required for θ-directional data is:

$$F(\theta) = \frac{(P_2-P_3)}{(P_3-P_1) + (P_2-P_1)}$$

$F(\theta)$ is plotted in Figs. 10-12 and is independent of ϕ for $\theta = \pm 30°$.

Once θ and ϕ have been obtained, freestream static and total pressure can be determined from the individual pressure transducer readings via calibration curves.

Pressure Transducer Used

The pressure transducers used are Diffused Silicon Diaphragms. They consist of a circular diaphragm, 0.058 inches in diameter and 0.001 inches thick and are cemented into machined seats on the probe sphere (Fig. 3). A wheatstone bridge circuit is deposited on the diaphragm and the local probe pressure measured is proportional to the voltage output of the bridge. The pressure transducers have a natural frequency in excess of 150 KHz.

II. PROBE CALIBRATION TECHNIQUE

Calibration Probe

The calibration curves were obtained from steady-state measurements in an open jet via a calibration probe. This probe had conventional pressure taps instead of the delicate Kulite pressure transducers and was twice fullscale (Fig. 4). For the steady-state pressure measurements, openend manometer boards were used. Oil (s.g. = 0.827) was used for low Mach number tests and Mercury (s.g. = 13.6) was used for high Mach number tests (M = 0.7, 0.9). The definitions of calibration angles are given in Fig. 4.

Using an Open Jet for Probe Calibration

An open jet consists of an inner jet core and a mixing region where viscous shearing forces decelerate and mix the jet with the surrounding medium (Fig. 5). A velocity profile of the 1" open jet used for probe calibration (Fig. 6), shows the jet core to be completely developed around 5 jet-diameters downstream. So that the calibration probe would not be subjected to jet velocity errors, a test plane 1 jet-diameter downstream was chosen for calibration measurements.

Another open jet property is jet spreading (Fig. 7). Schlichting[7] develops the exact solution for a turbulent circular jet and determines the dimensionless constants required to describe the jet. One empirical relationship describes the spreading phenomenon,

$$b_{1/2} = 0.0848\ x$$

where $b_{1/2}$ is 1/2 jet width at a given downstream location, x. Schlichting

shows the jet width is proportional to x, therefore, the included angle of jet spreading is,

$$\tan^{-1} [2 \times (0.0848)] = 10.77°$$

Experimental verification of the jet streamline spreading is shown in Fig. 8 where a detailed directional survey of the 3-inch open jet, obtained with the sphere probe, is plotted for a station 1-inch downstream of the orifice. The streamlines within the jet core boundaries were found to spread at approximately 10.8°.

Open Jet Error Sources

Probe calibration errors can occur from jet core streamline curvature and poor probe positioning in the jet core. To minimize these error sources, the calibration probe must remain in the same jet core position for different θ and ϕ orientations. To accomplish this, an alignment laser was used.

A second large error source originates from probe blockage in the open jet (Fig. 9). This error is caused by the open jet being forced to bulge around the probe body. This bulging causes a local velocity error consisting of a lower maximum increase in local probe velocity with an open jet than with an infinitely wide freestream. According to Ref. 8, the exact solution for the maximum local velocity of a cylinder in a two-dimensional jet is:

$$\frac{V_{MAX}}{V_{jet}} = 2 + 7/6\ M_{jet}^{2} - \frac{\pi^2}{12}\left(\frac{d}{H}\right)^2\left(1 + \frac{43}{12} M_{jet}^{2}\right) + \ldots$$

where d is the cylinder diameter and H is the jet width. The maximum bulge width, W_{MAX}, is:

$$\frac{W_{MAX} - H}{H} = \frac{\pi}{2}\left(\frac{d}{H}\right)^2\left(1 + \frac{5}{6} M_{jet}^2\right) + \ldots .$$

For increasing values of d/H, V_{MAX}/V_{jet} decreases. Because $C_{P_n} = 1 - (V_{local}/V_{jet})^2$, a significant dependence between local probe pressure and d/H occurs if d/H is sufficiently large. All calibration curves were done in the 1" open jet and d/H had a value of approximately 0.25 to 0.35.

The significance of probe blockage error in the open jet calibrations depends upon the calibration function. The error is insignificant if it cancels out of the calibration function, such as in the directional calibrations. A velocity error calculation due to probe blockage done with the above equation for a cylinder in a two-dimensional jet with d/H = 0.35 and $M_{jet} = 0.27$, gives a velocity error of 6.7%.

Zero Angle Reference Pressure Distribution

Because of discrepancies in experimental apparatus (streamline curvature, jet core position, etc.), a reference pressure distribution where $P_2 = P_3 = P_4$ was chosen to define 0° θ and 0° ϕ regardless of stem orientation to freestream direction. To duplicate probe pressure measurements, probe orientation angles must be measured from a reference pressure distribution instead of a mechanical reference. This eliminated day to day discrepancies in experimental apparatus because the freestream flow only came from one direction when $P_2 = P_3 = P_4$.

III. PROBE CALIBRATION CURVES

$F(\theta,M)$, $F(\phi,M)$	- Directional Calibration Curves
$H(\theta,\phi,M)$	- Dynamic Head (total-static pressure) Calibration Curves
$K_{P_n}(\theta,\phi,M)$	- Static Pressure Calibration Curves
M	- Freestream Mach Number
P_n	- Absolute Pressure Retrieved by Pressure Transducers
P_s	- Freestream Static Pressure
$(P_T - P_s)$	- Freestream Dynamic Head (freestream total-static pressure)
θ,ϕ	- Freestream Rotational and Radial Angles

The following calibration curves are plotted with techniques which minimize data processing required to retrieve freestream total and static pressure, and freestream flow angles. These techniques consist of using absolute probe pressures, interpolation, and calibration functions which are only a function of the desired flow direction. For example, the θ-directional calibrations, $F(\theta,M)$(Figs. 10-12), are mainly a function of θ, nearly independent of ϕ. Calibration curves are plotted for $M = 0.27$, 0.7, and 0.9. Comparison of them shows there is almost no Mach number dependence. The plotted calibration points are catalogued in the Appendix.

Retrieving Freestream θ and ϕ from Directional Calibrations

To facilitate freestream directional data retrieval, calibration curves should be a function of only one flow angle. The required calibration functions are:

$$F(\theta,M) = \frac{(P_2-P_3)}{[(P_2-P_1) + (P_3-P_1)]}$$

$$-20° \leq \theta \leq +20°$$

$$F(\phi,M) = \frac{(P_4-P_5)}{[(P_4-P_1) + (P_5-P_1)]}$$

$$-20° \leq \phi \leq +20°$$

$F(\theta,M)$ calibration curves are plotted in Figs. 10, 11, and 12 for Mach numbers of 0.27, 0.7, and 0.9. The functions are plotted over ± 40° although a usable range of ± 20° is recommended. These directional calibrations are almost independent of ϕ and Mach number.

The $F(\phi,M)$ calibration curves are plotted in Figs. 13 and 14 for corresponding Mach numbers of 0.27 and 0.7. The normalization error (curve spread at large angles of ϕ and zero shift) in these plots is due to stem effect on P_5 which reduces the probes ϕ directional sensitivity (P_4-P_5). To make up for the reduced sensitivity at large angles of ϕ, interpolation between the curves for $\theta = \pm 20°$ and $\theta = 0°$ with the retrieved freestream θ is required. Directional calibrations in the ϕ direction are also nearly independent of Mach number.

Retrieving Freestream Dynamic Head

To retrieve freestream dynamic head (Freestream total-static pressure), the following calibration function is used.

$$H(\theta,\phi,M) = \frac{(P_T-P_s)}{[(P_2-P_1) + (P_3-P_1)]}$$

$$-20° \leq \theta \leq +20° \qquad -20° \leq \phi \leq +20°$$

The freestream dynamic head is

$$(P_T - P_s) = H(\theta,\phi,M) \cdot \left[(P_2 - P_1) + (P_3 - P_1)\right]$$

where the pressures inside the square brackets are absolute pressures retrieved from the probe. $H(\theta,\phi,M)$ is plotted for M = 0.27, 0.7, and 0.9 in Figs. 15, 16, and 17. $H(\theta,\phi,M)$ is always negative because the quantity $\left[(P_2 - P_1) + (P_3 - P_1)\right]$ is always negative .

Retrieving Freestream Static Pressure

To retrieve freestream static pressure, the following calibration function is used.

$$K_{P_n}(\theta,\phi,M) = \frac{(P_n - P_s)}{\left[(P_2 - P_1) + (P_3 - P_1)\right]}$$

$$-20° \leq \theta \leq +20° \qquad -20° \leq \phi \leq +20°$$

The local freestream static pressure is

$$P_s = P_n - K_{P_n}(\theta,\phi,M) \cdot \left[(P_2 - P_1) + (P_3 - P_1)\right]$$

Because P_2, or P_3 both retrieve excellent pressure data, either could be used for retrieving freestream static pressure depending upon which diaphragm is best oriented to measure the pressure ($P_S \simeq P_n$ etc).

$$P_s = P_2 - K_{P_2}(\theta,\phi,M) \cdot \left[(P_2 - P_1) + (P_3 - P_1)\right] \quad (\theta > 0°)$$

or

$$P_s = P_3 - K_{P_3}(\theta,\phi,M) \cdot \left[(P_2 - P_1) + (P_3 - P_1)\right] \quad (\theta < 0°)$$

Because P_1 essentially measures total pressure, K_{P_1} is also plotted to measure total head variations due to angle of attack. K_{P_1} is required to retrieve accurate total pressure measurements.

The static pressure calibration functions K_{P_1}, K_{P_2} and K_{P_3} are plotted in Figs. 18, 19 and 20 for M = 0.7. For retrieving data at other Mach numbers, K_{P_2} is plotted in Figs. 21 and 22 for M = 0.27 and 0.9.

Retrieving Freestream Total Pressure

The freestream total pressure is equal to the freestream dynamic head, $P_T - P_S$, plus static pressure, P_S. To minimize errors in the total pressure retrieval, K_{P_1} is used for static pressure retrieval because P_1 essentially measures P_T over most angles of attack.

$$P_T = H(\theta,\phi,M)[(P_2-P_1) + (P_3-P_1)] + P_S$$

$$P_T = P_1 + [H(\theta,\phi,M) - K_{P_1}(\theta,\phi,M)] \cdot [(P_2-P_1) + (P_3-P_1)]$$

For small angles of attack $[H(\theta,\phi,M) - K_{P_1}(\theta,\phi,M)]$ is essentially zero or:

$$P_T \simeq P_1$$

Interpolation for Total and Static Pressure Calibration Factors

In addition to finding the total and static pressure calibration factors $[H(\theta,\phi,M)$ and $K_{P_n}(\theta,\phi,M)]$ with the retrieved freestream θ, a linear interpolation with the retrieved freestream ϕ is required for an accurate total or static pressure calibration factor. This linear ϕ interpolation consists of linearly interpolating between $\phi = 0°$ and $\phi = \pm 25°$ or $\pm 20°$ on the $H(\theta,\phi,M)$ and $K_{P_n}(\theta,\phi,M)$ calibration curves with the retrieved freestream ϕ.

IV. PROBE OPERATING LIMITATIONS

Local probe pressure coefficients [$C_{p_n} = (P_n - P_s)/(P_T - P_s)$] are used to examine probe directional, Mach number, and Reynolds number limitations.

Directional Limitations

P_1 had the best angle of attack range of all 5 probe pressures and retrieved accurate data over the probes usable angle of attack range ± 20° θ and ± 20° ϕ. A plot of C_{P_1} over ± 40° θ is shown in Fig. 23. The data looked similar for C_{P_1} values over the usable ϕ range.

Due to flow separation, the range for P_2 was limited to 20° θ and was limited for P_3 to -20° θ, thus, defining the usable ± 20° θ range (Figs. 24 and 25). Similar behavior was observed for P_4 over the range of radial flow angle, ϕ = ± 20° (Fig. 26). The large probe stem effect at the P_5 location can be seen by comparing Figs. 26 and 27. The early fall off of the P_5 pressure coefficient at ϕ = ± 20° reduces the radial directional sensitivity but does not unduly complicate the data reduction process.

Mach Number Dependence

P_1 exhibited a small Mach number dependence over the usable angle of attack range of θ = ± 20° and ϕ = ± 20° (Fig. 23). The Mach number dependence is small because the freestream flow is essentially stagnated at P_1 over this angle of attack range.

P_2, P_3, P_4, and P_5 had a significant freestream Mach number dependence for θ = ± 20° and ϕ = ± 20°. This Mach number dependence took the form of increasing C_p values for increasing freestream Mach numbers (Figs. 24-28). This Mach number dependence has two possible explanations. The first

explanation suggests the increasing pressure coefficients are just compressible flow effects from the high subsonic freestream Mach numbers ($0.27 \leq M \leq 0.9$). The other explanation for the Mach number dependence is the probe blockage velocity error discussed in "Open Jet Error Sources". The Mach number dependence is probably a superposition of both effects.

Critical Mach Number Limitations

The local probe pressure coefficient must be calculated before finding the critical Mach number.

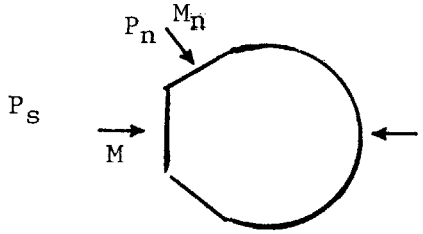

P_n = Local probe pressure
M_n = Local probe Mach number
P_s = Freestream static pressure
M = Freestream Mach number

The following compressible flow relationships are needed from Ref. 5.

1. $P_T/P_s = \left(1 + \frac{\gamma-1}{2} \cdot M^2\right)^{\frac{\gamma}{\gamma-1}}$

2. $P_T/P_n = \left(1 + \frac{\gamma-1}{2} \cdot M_n^2\right)^{\frac{\gamma}{\gamma-1}}$

3. $C_{pn} = \left(P_n - P_s\right)/\left(P_t - P_s\right) = \left(P_n/P_s - 1\right) 2/\gamma M^2$

$$C_{pn} = \left[\left(\frac{1 + [(\gamma - 1)/2] M^2}{1 + [(\gamma - 1)/2] M_n^2}\right)^{\gamma/\gamma-1} - 1\right] \cdot 2/\gamma M^2$$

The critical pressure coefficient is defined as that for a local probe Mach number of 1 ($M_n = 1$).

$$C_{p\ crit} = \left[\left(\frac{2}{\gamma + 1} + \frac{\gamma - 1}{\gamma + 1} \cdot M^2\right)^{\gamma/\gamma-1} - 1\right] \cdot 2/\gamma M^2$$

The following critical pressure coefficient values are obtained for various freestream Mach numbers

M	0.7	0.75	0.8	0.85	0.9
$C_{p_{crit}}$	-0.779	-0.591	-0.435	-0.302	-0.188

No pressure coefficients appear significantly below zero in Figs. 24 and 25 for the range of Mach numbers tested and the usable θ range, thus establishing the useful maximum Mach number at about 0.90.

Errors in Estimation of Critical Mach Number

If the previous relationship between freestream Mach number and $C_{p_{crit}}$ is valid, then the only error source occurs in estimating $C_{p_{crit}}$ from the experimental data (Figs. 24 and 25). The lowest possible value for C_p in Figs. 24 and 25 is -0.6 and setting this equal to $C_{p_{crit}}$ gives a conservative estimation of critical Mach number. This is not a bad estimate because $C_{p_{MIN}}$ did not vary significantly for freestream Mach numbers of 0.27 to 0.9.

Directly measuring the exact critical Mach number is difficult because of the probe blockage velocity error discussed in Open Jet Error Sources. This velocity error delays any shock formation beyond the actual critical Mach number in an indinite freestream.

Reynolds Number Independence

The pressure coefficients were essentially independent of Reynolds number over a range of 14,000 to 92,000 (Figs. 29, 30, 31), the variations at large θ being attributed to open jet bulge error. Because of the impossibility for a laminar boundary-layer to occur at a Reynolds number of 92,000 for an imperfect sphere in a turbulent jet, the boundary layers appear to be turbulent over the useful range of Reynolds number.

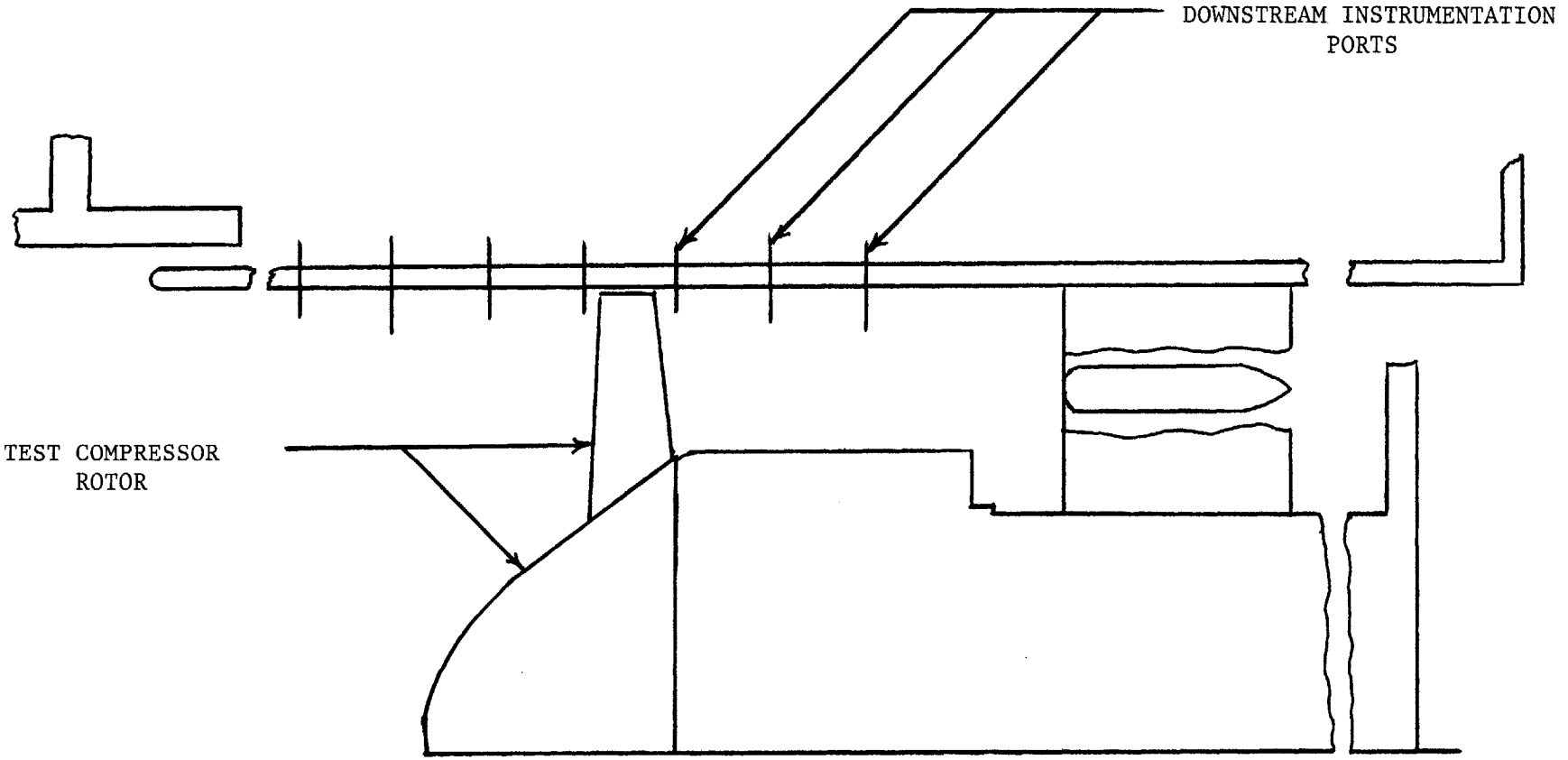

FIG. 1 - TEST SECTION - MIT COMPRESSOR FACILITY

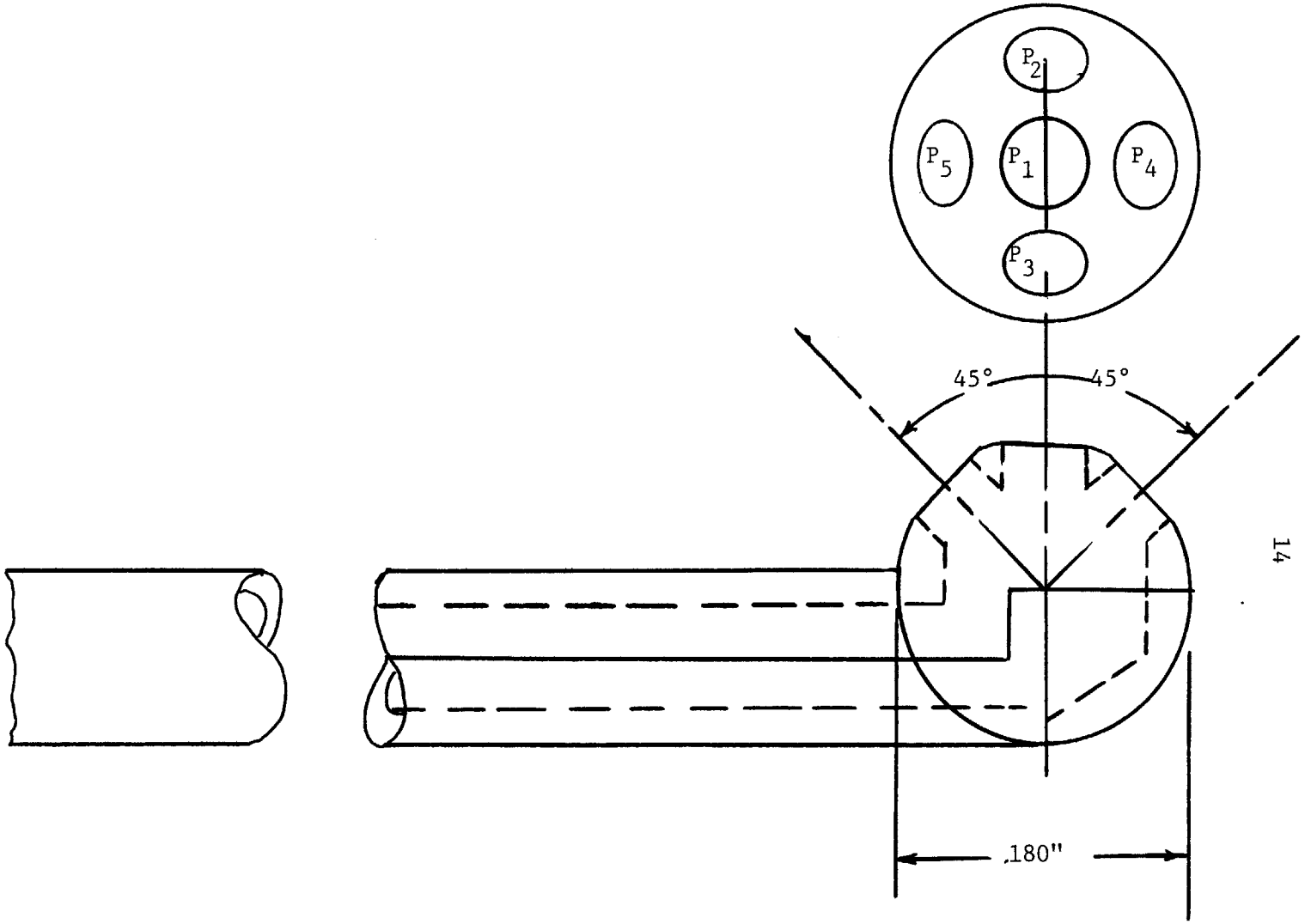

FIG. 2 - COMPRESSOR FACILITY DIRECTIONAL PROBE

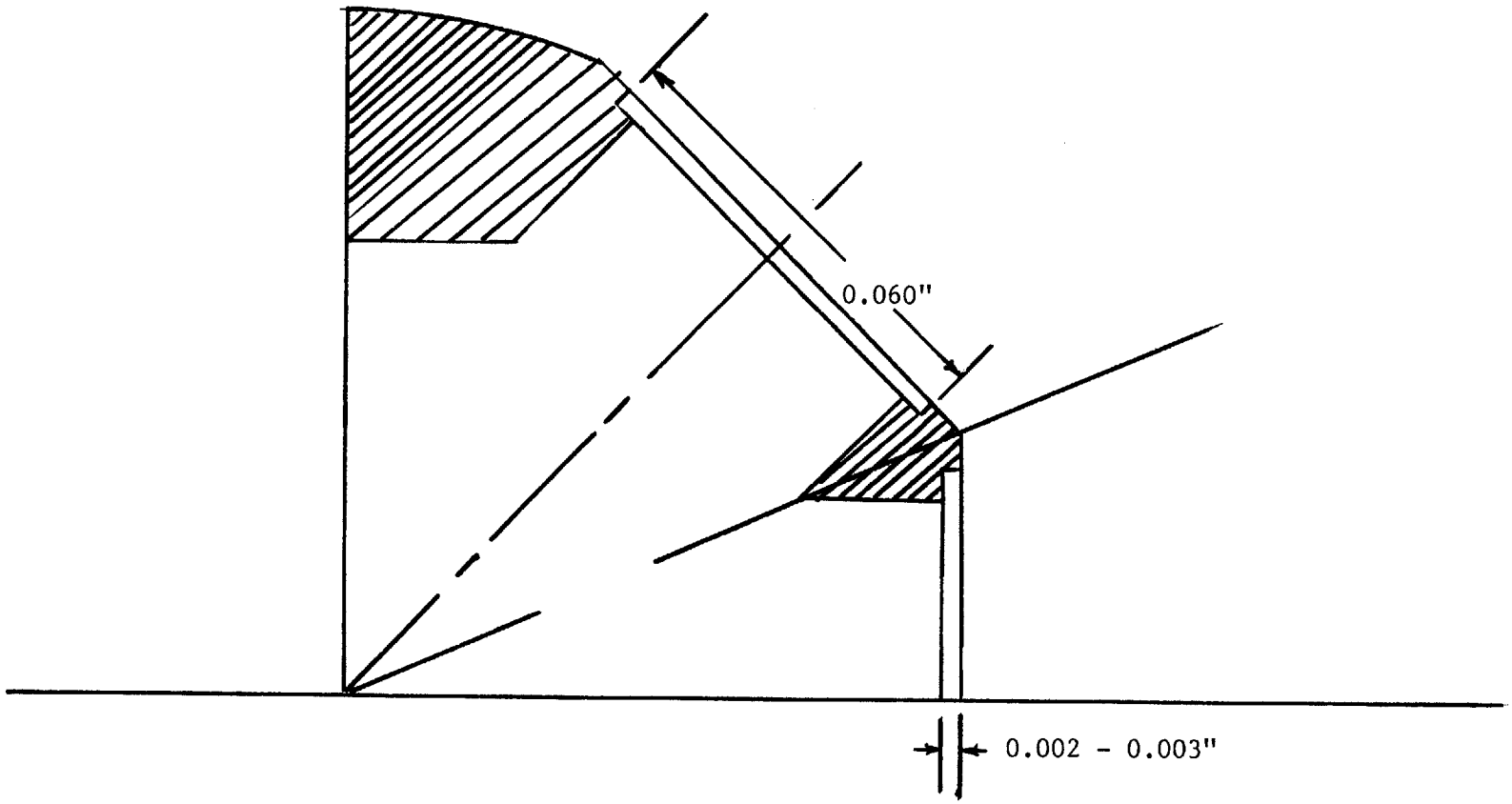

FIG. 3 - DIAPHRAGM WELLS (KULITE PRESSURE DIAPHRAGMS)
= 0.058" x 0.001"

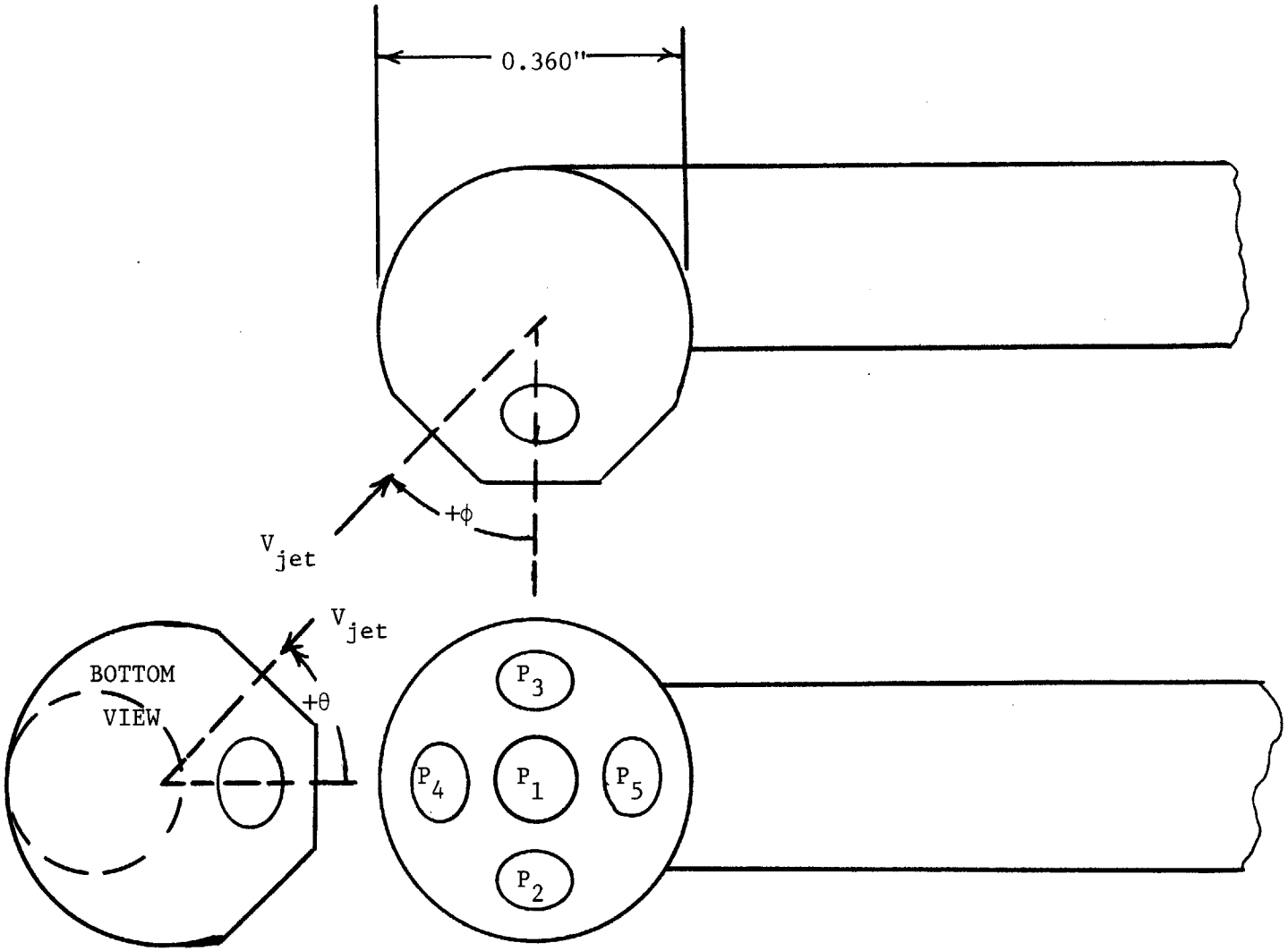

FIG. 4 - CALIBRATION PROBE - ANGLE DEFINITIONS AND PRESSURE TAP LABELS

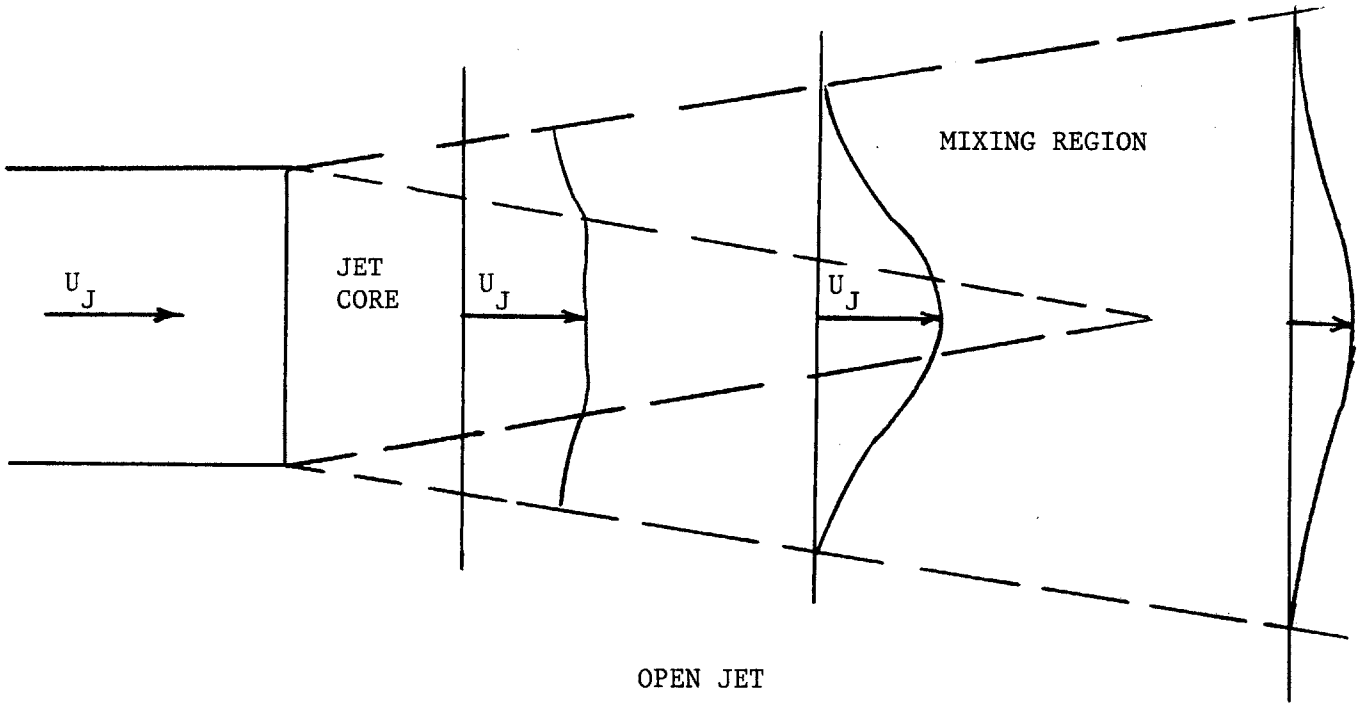

OPEN JET

FIG. 5

FIG. 6 - OPEN JET CALIBRATION
(1 JET AND 3 JET DIAMETERS DOWNSTREAM)
JET DIAMETER = 1 INCH

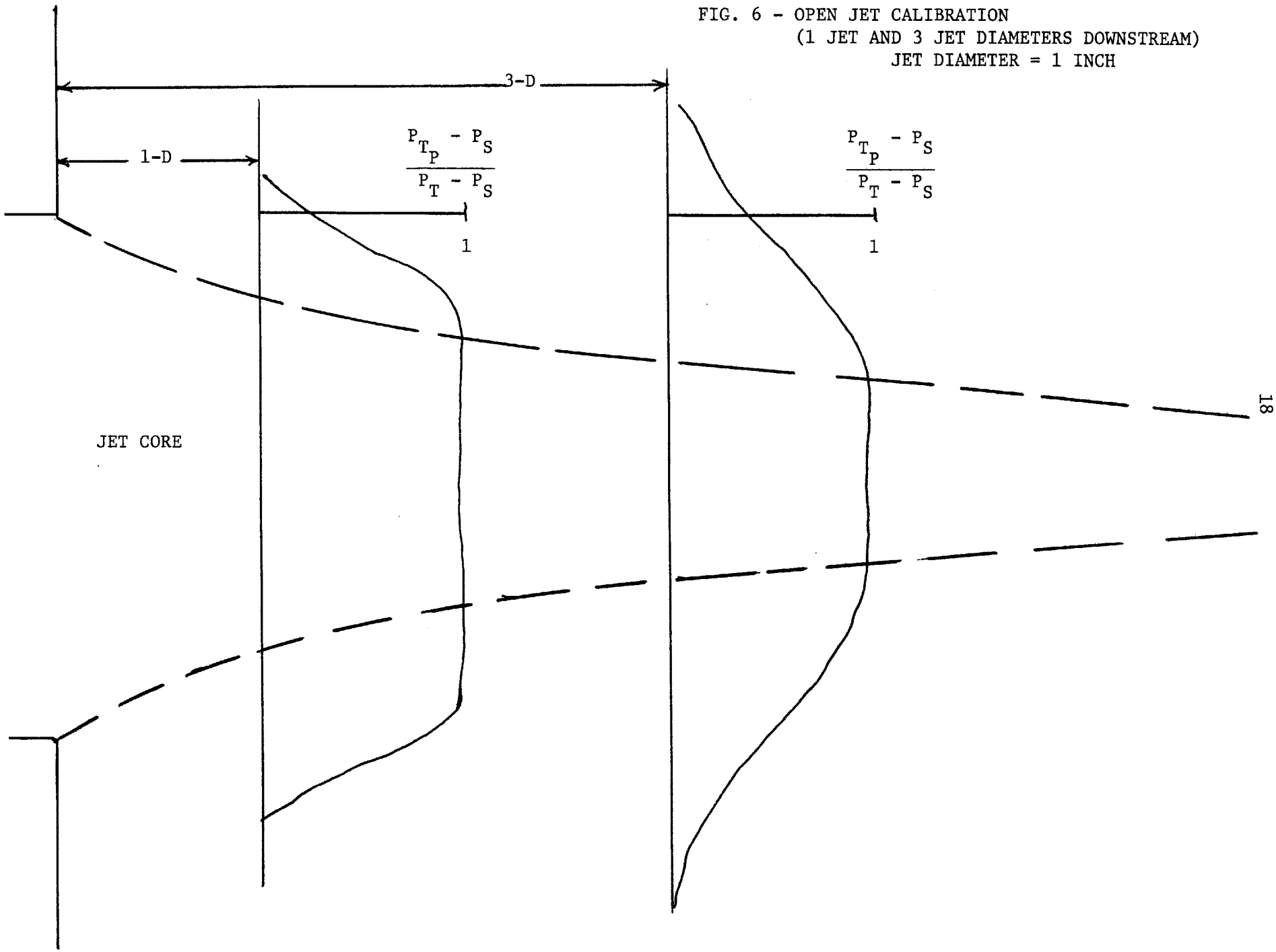

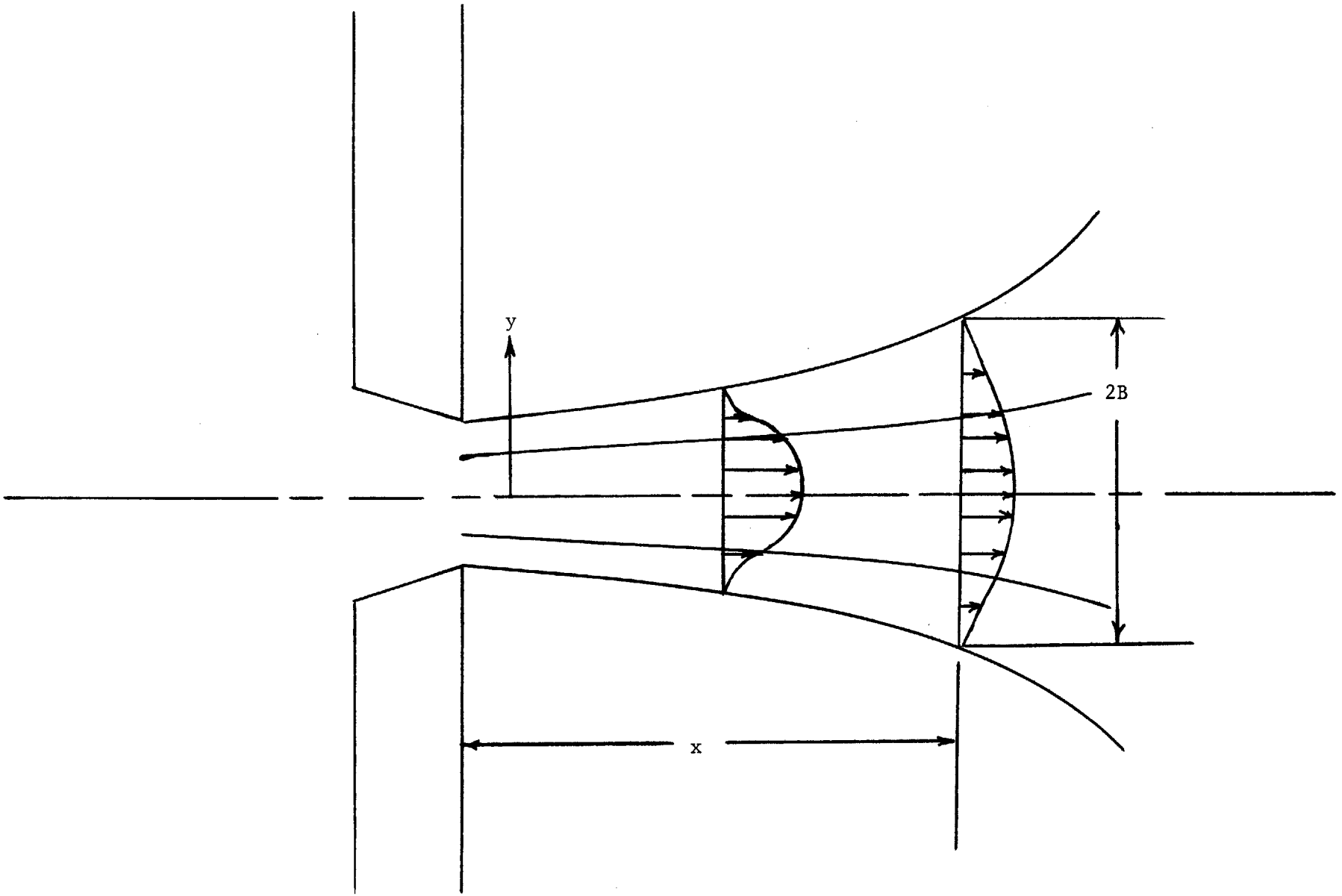

FIG. 7 - JET SPREADING

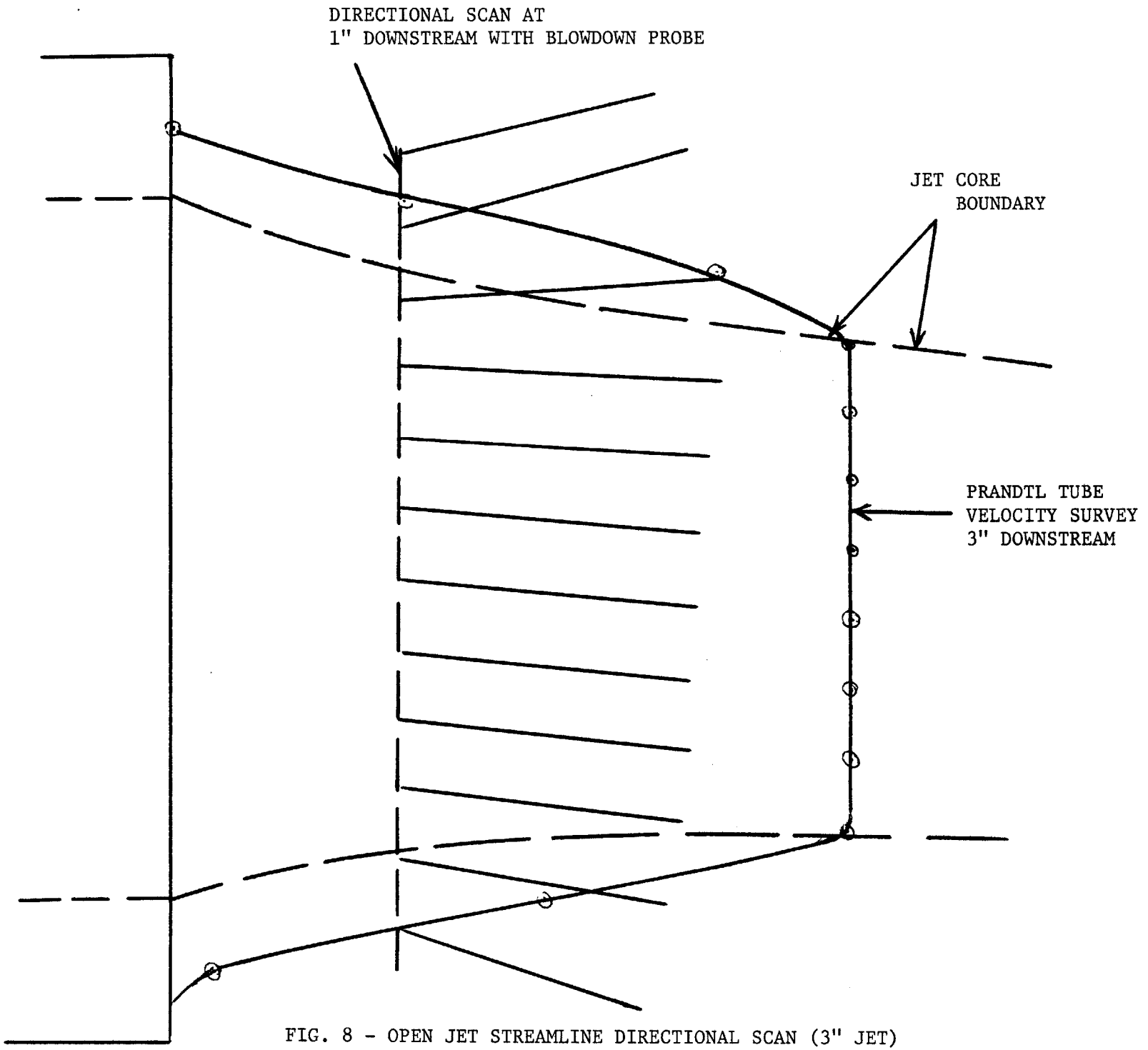

FIG. 8 - OPEN JET STREAMLINE DIRECTIONAL SCAN (3" JET)

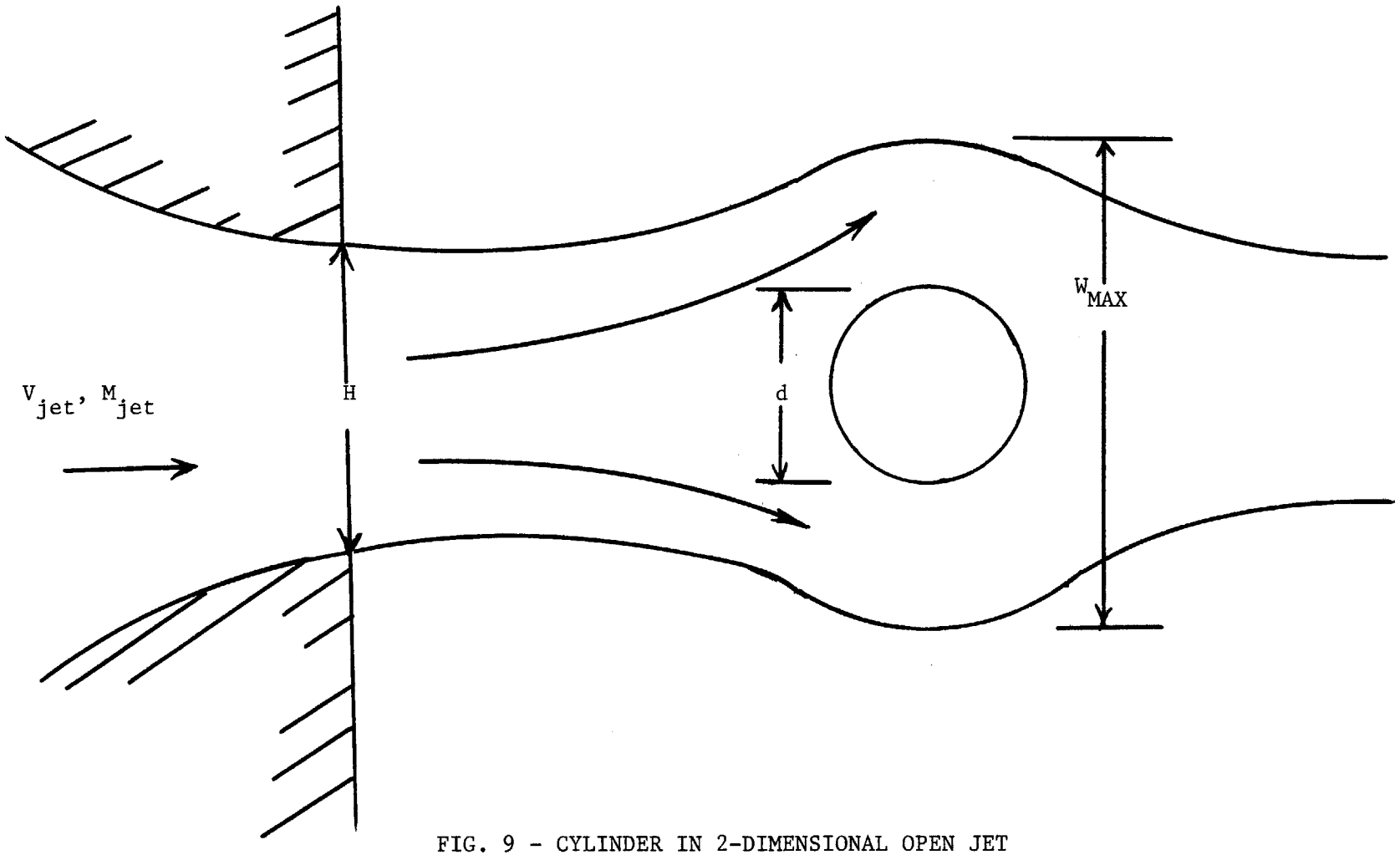

FIG. 9 - CYLINDER IN 2-DIMENSIONAL OPEN JET

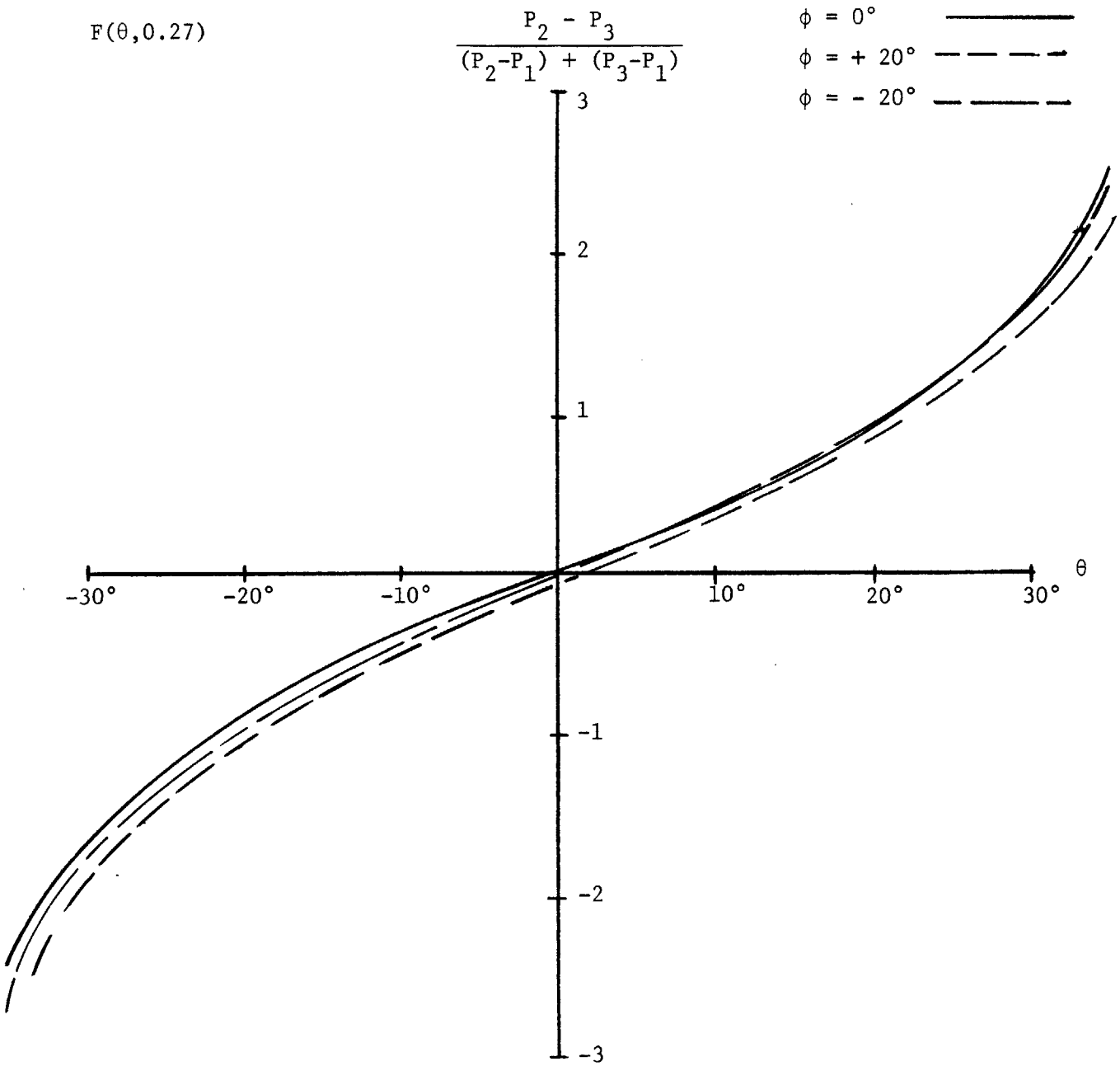

FIG. 10 - θ DIRECTIONAL CALIBRATION (M = 0.27)

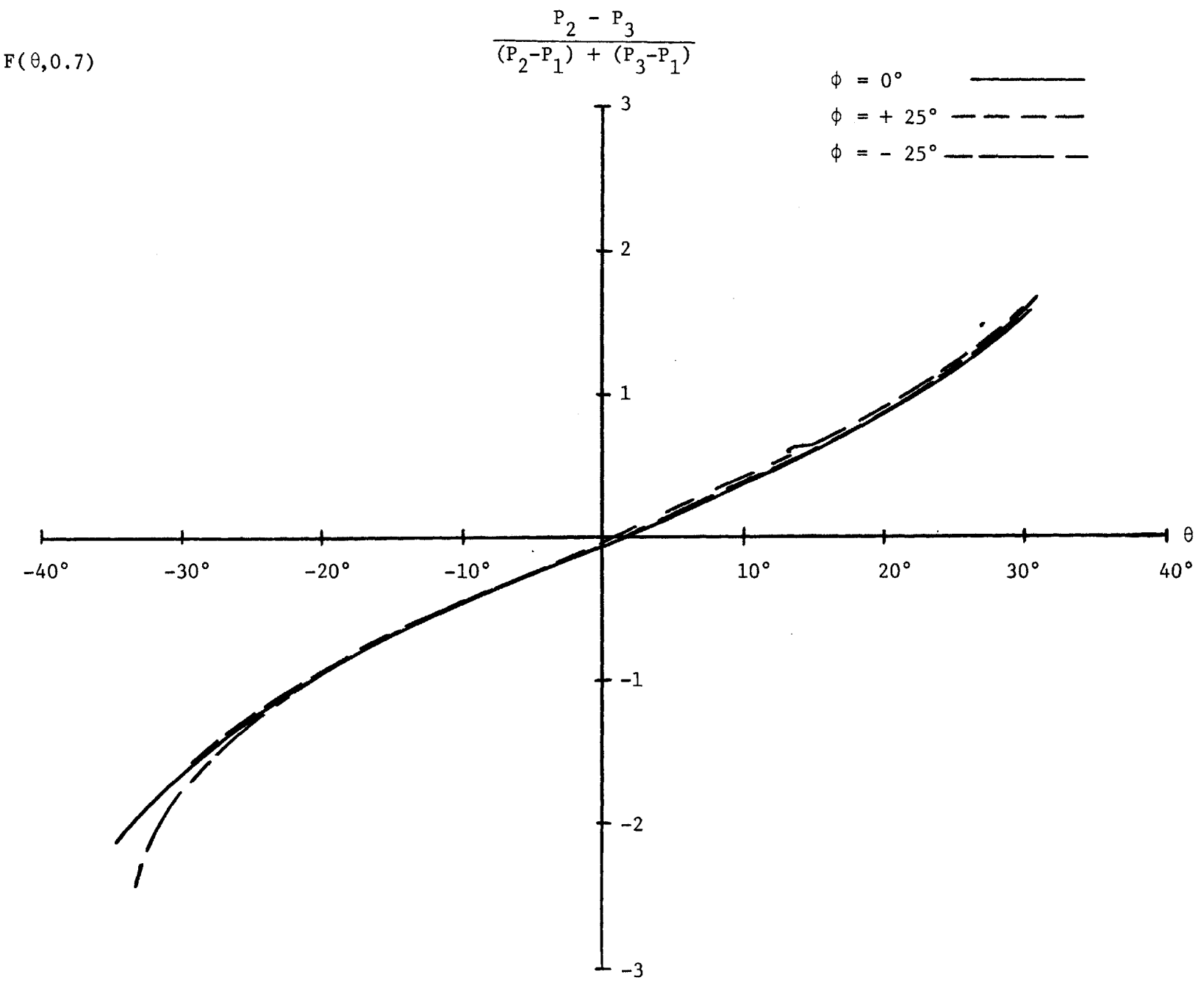

FIG. 11 - θ DIRECTIONAL CALIBRATION (M = 0.7)

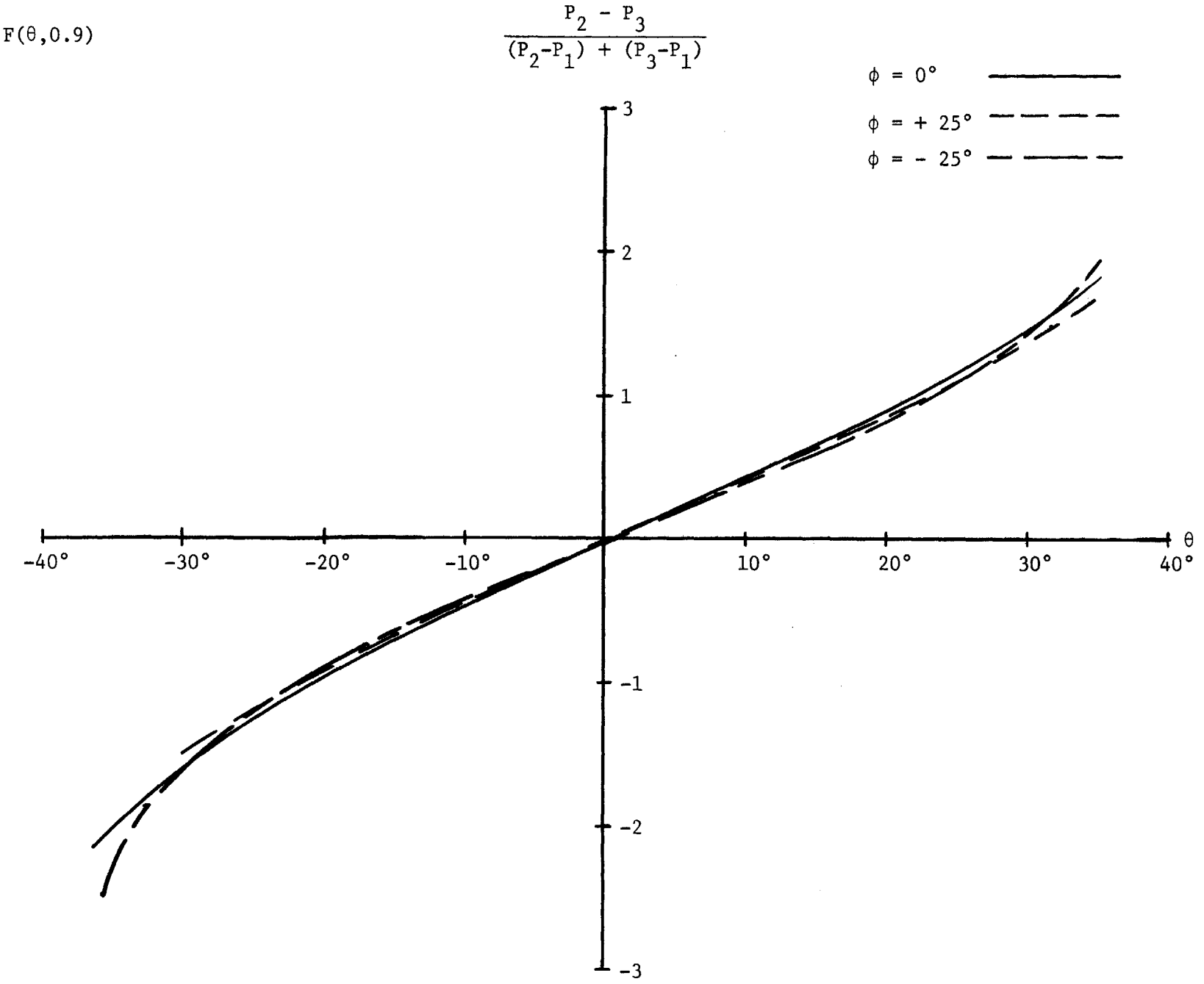

FIG. 12 - θ DIRECTIONAL CALIBRATION (M = 0.9)

$$F(\phi,0.27) \qquad \frac{P_4 - P_5}{(P_5-P_1) + (P_4-P_1)}$$

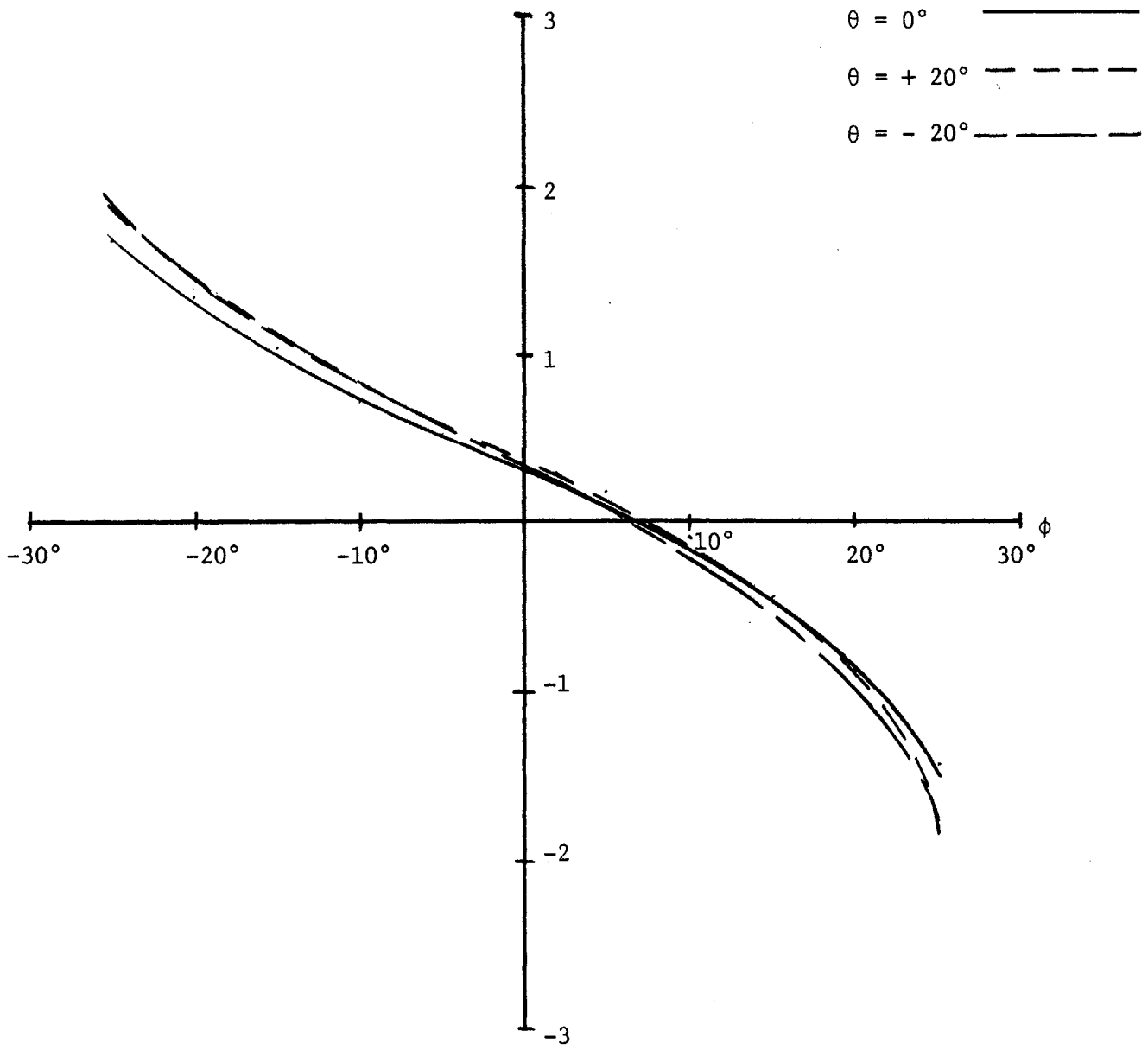

FIG. 13 - ϕ DIRECTIONAL CALIBRATION (M = 0.27)

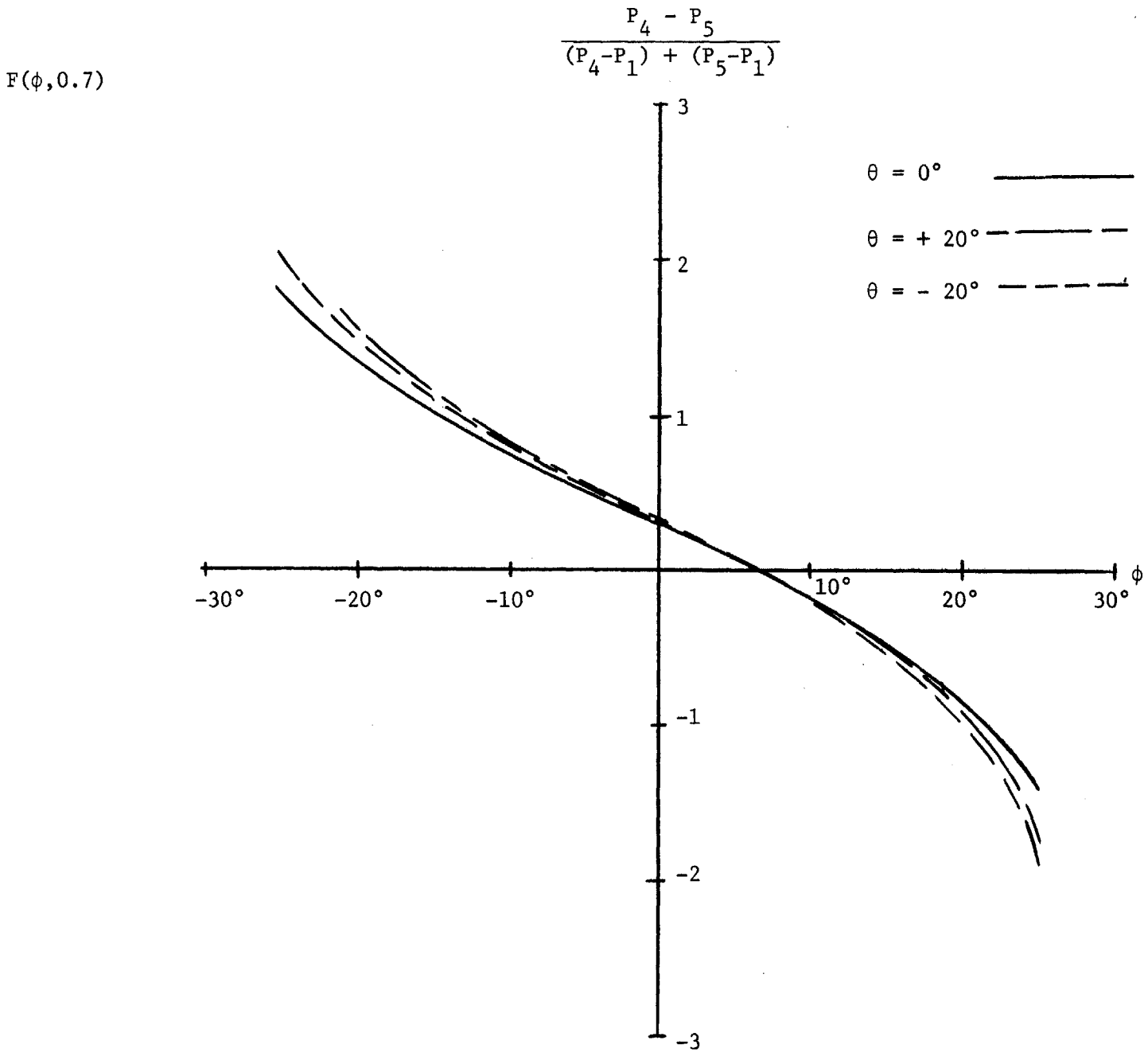

FIG. 14 - ϕ DIRECTIONAL CALIBRATION (M = 0.7)

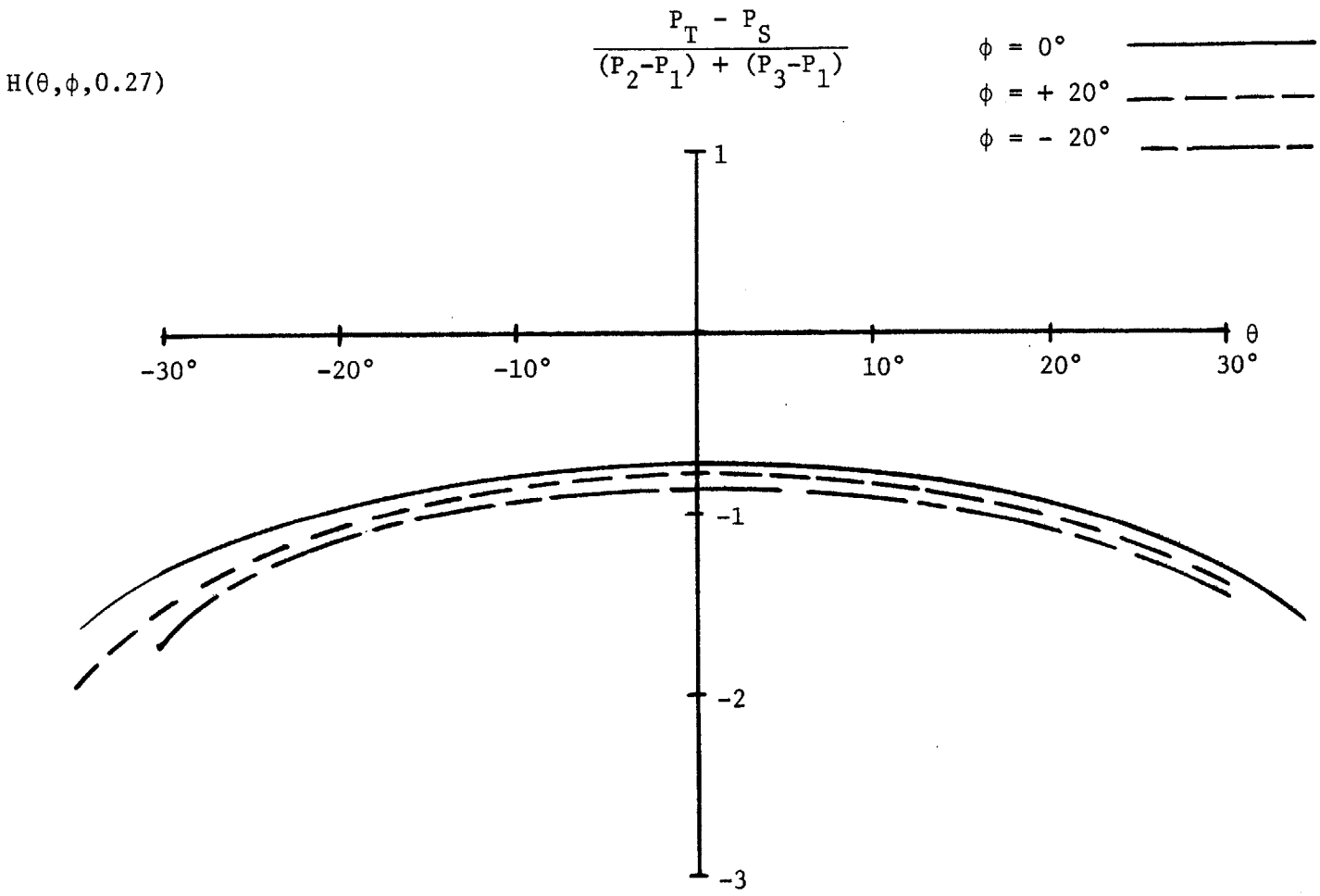

FIG. 15 - TOTAL PRESSURE CALIBRATION (M = 0.27)

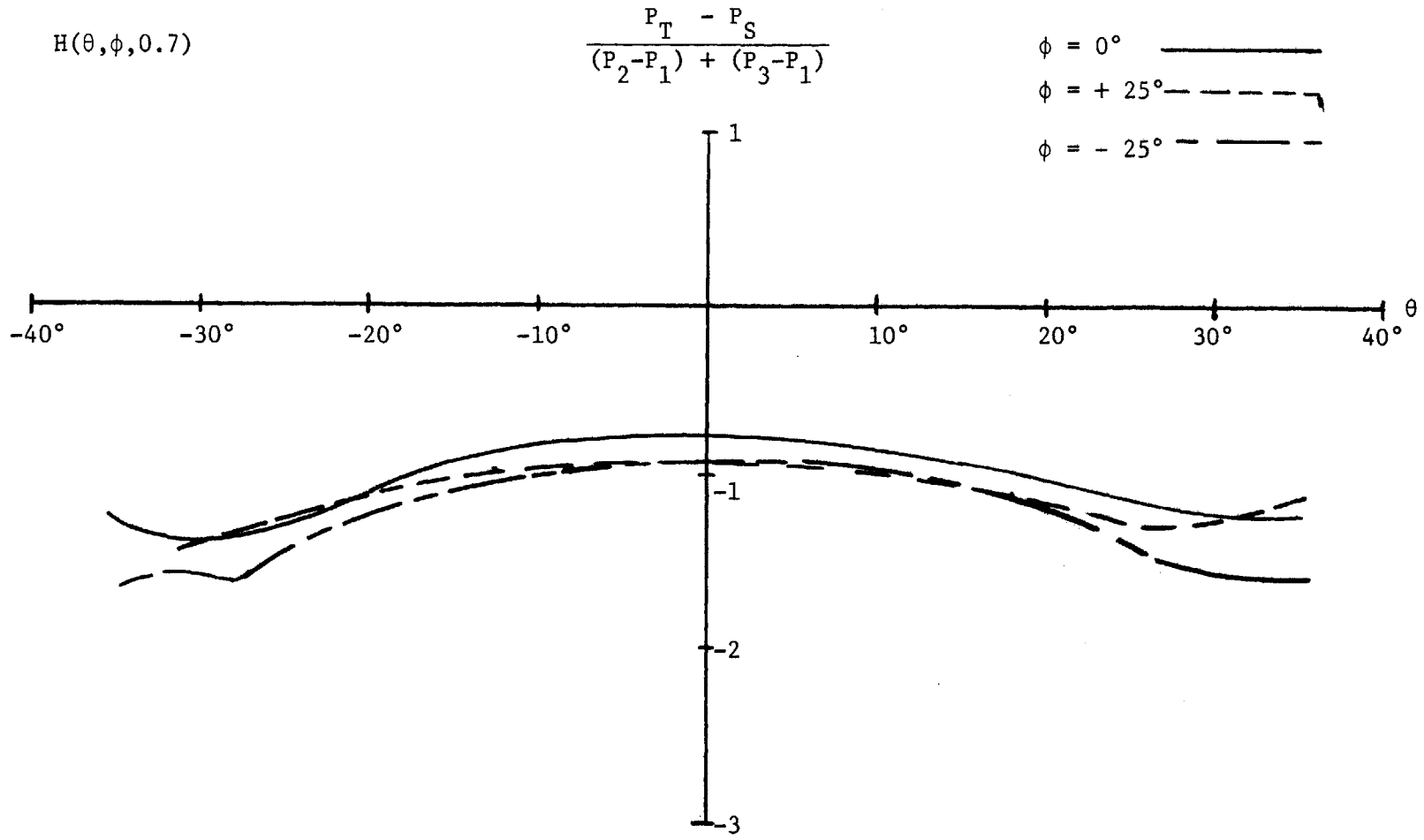

FIG. 16 - TOTAL PRESSURE CALIBRATION (M = 0.7)

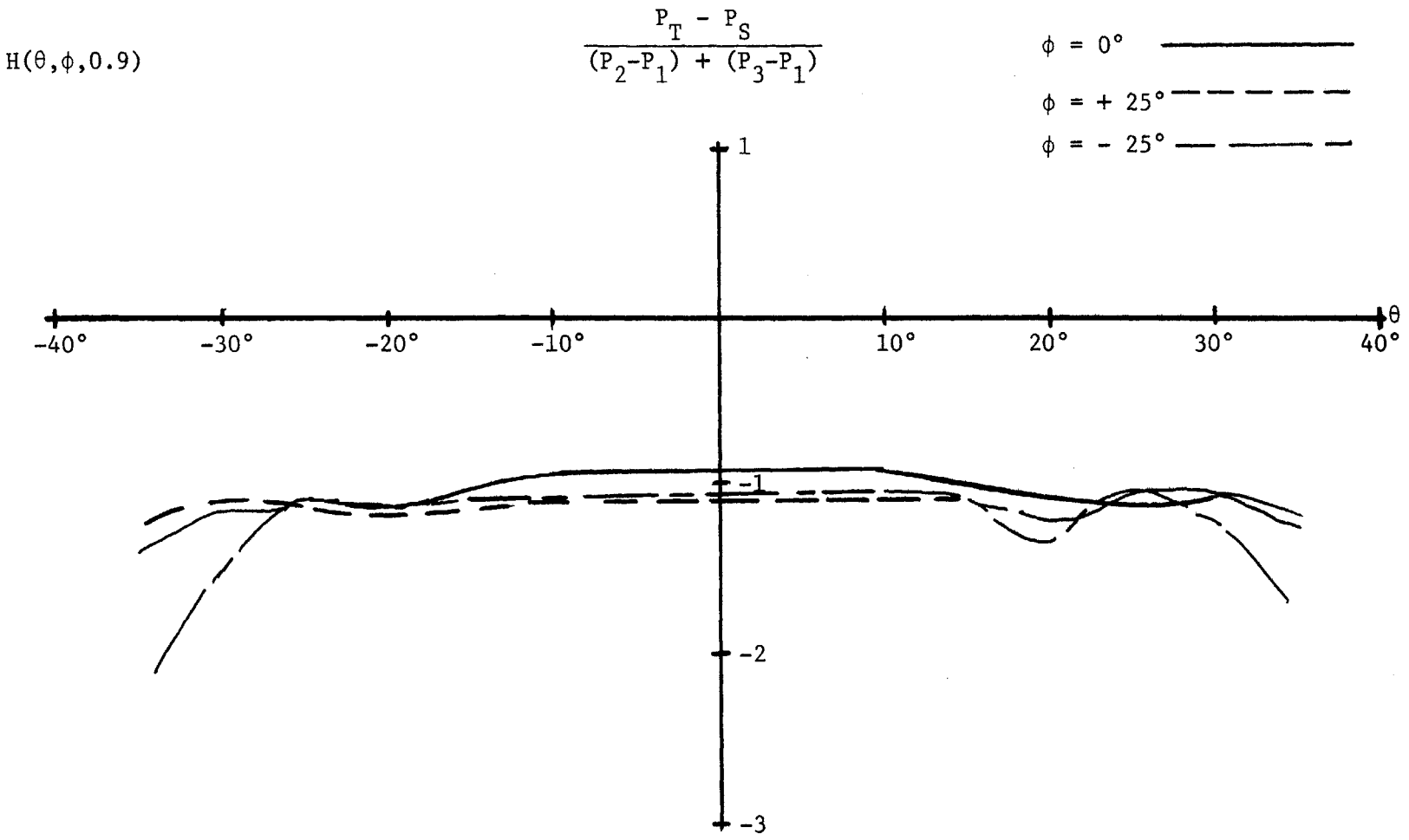

FIG. 17 - TOTAL PRESSURE CALIBRATION (M = 0.9)

$K_{P_1}(\theta,\phi,0.7)$ $\quad \dfrac{P_1 - P_S}{(P_2-P_1) + (P_3-P_1)}$

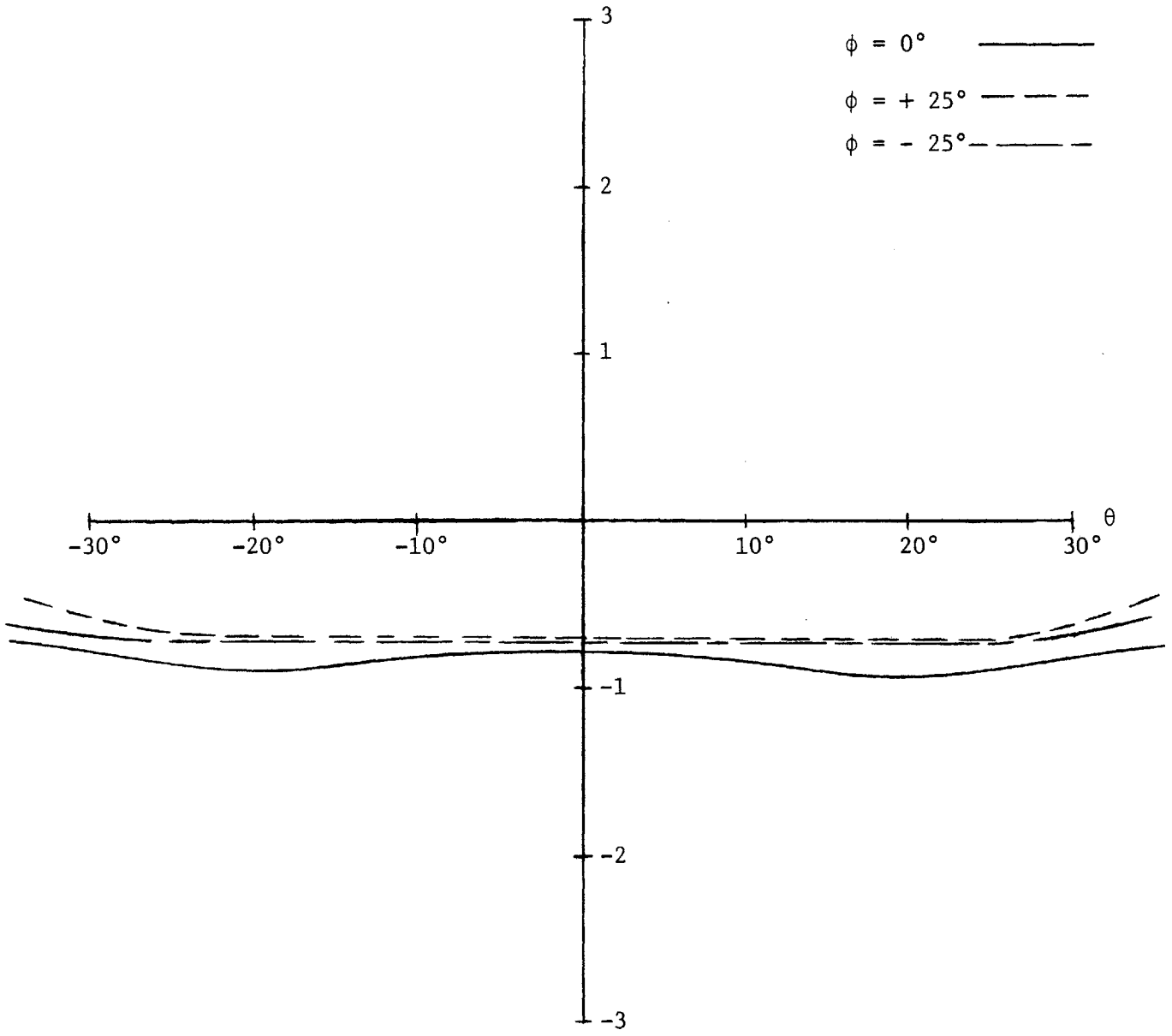

FIG. 18 - P_1 STATIC PRESSURE CALIBRATION (M = 0.7)

$$K_{P_2}(\theta,\phi,0.7) \qquad \frac{P_2 - P_S}{(P_2-P_1) + (P_3-P_1)}$$

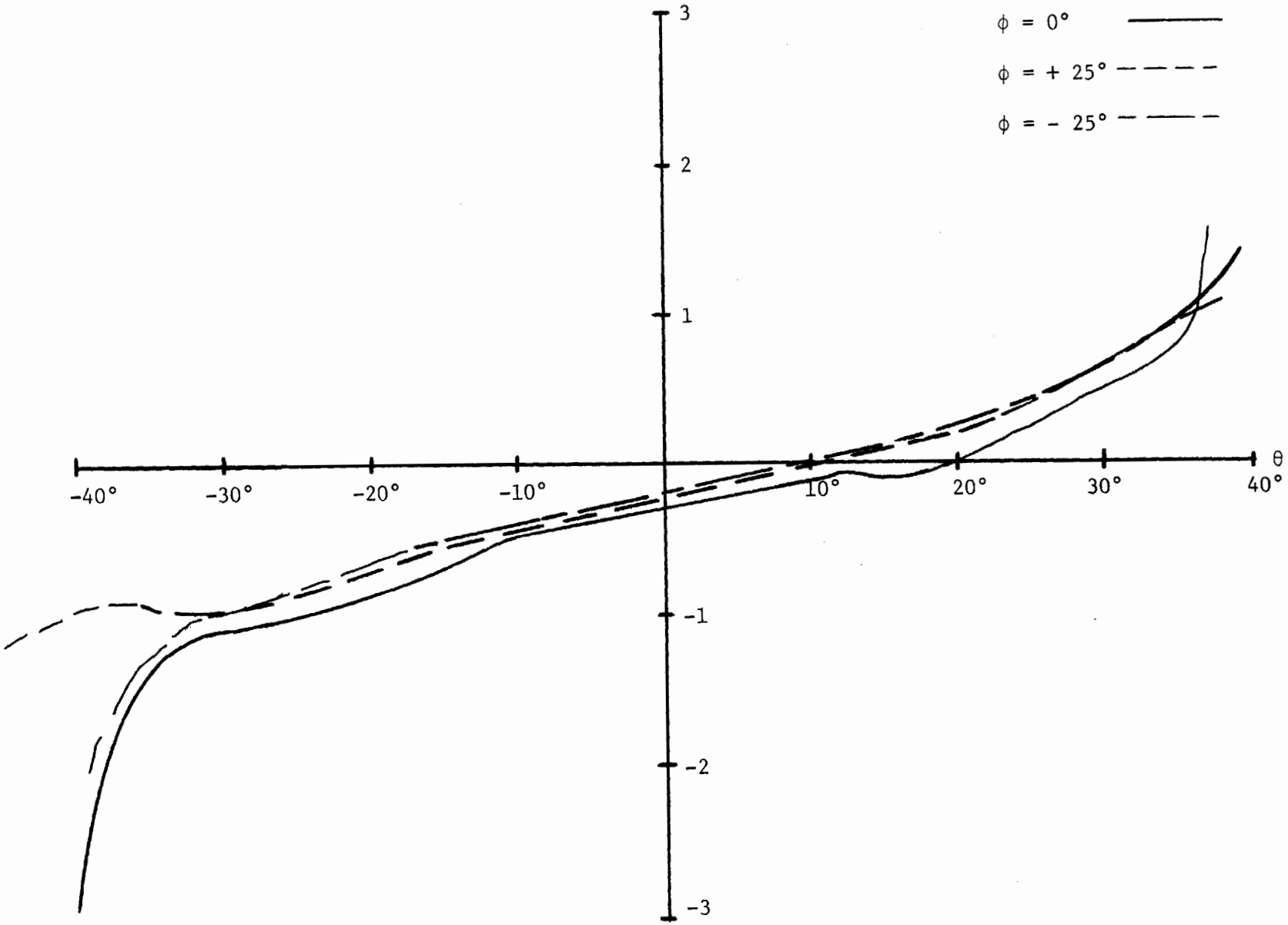

FIG. 19 - P_2 STATIC PRESSURE CALIBRATION (M = 0.7)

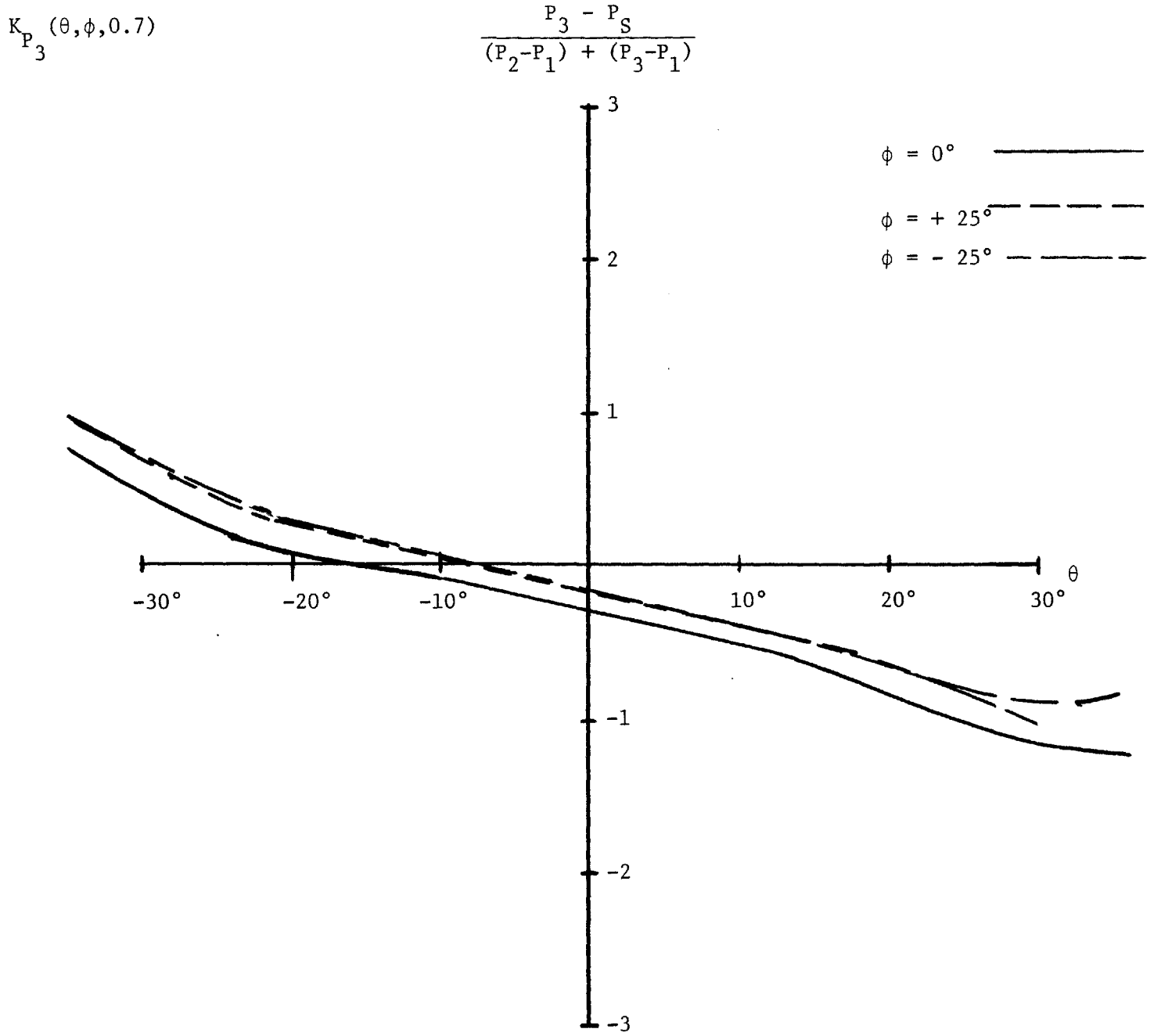

FIG. 20 - P_3 STATIC PRESSURE CALIBRATION (M = 0.7)

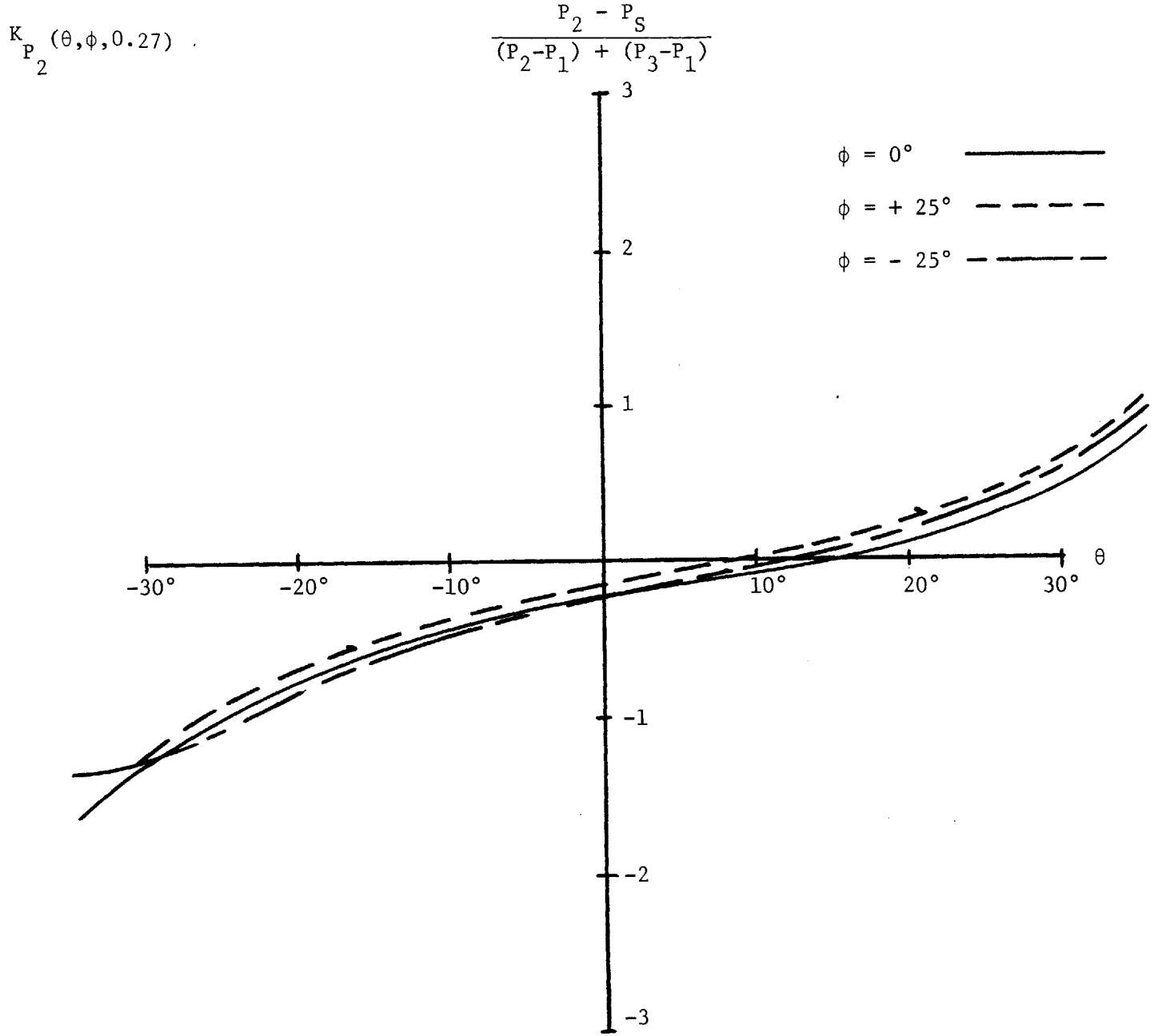

FIG. 21 - P_2 STATIC PRESSURE CALIBRATION (M = 0.27)

$$K_{P_2}(\theta,\phi,0.9) = \frac{P_2 - P_S}{(P_2-P_1) + (P_3-P_1)}$$

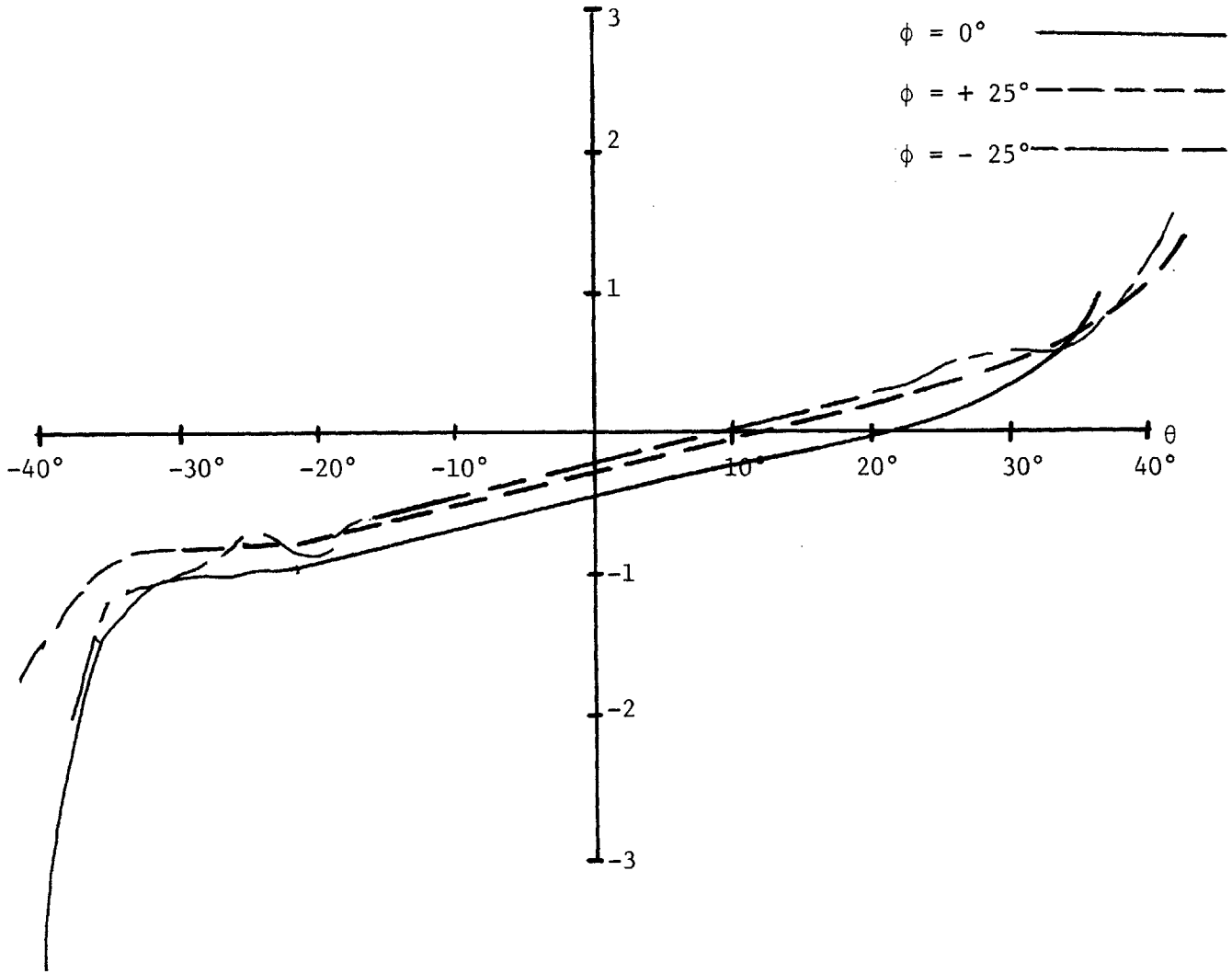

FIG. 22 - P_2 STATIC PRESSURE CALIBRATION (M = 0.9)

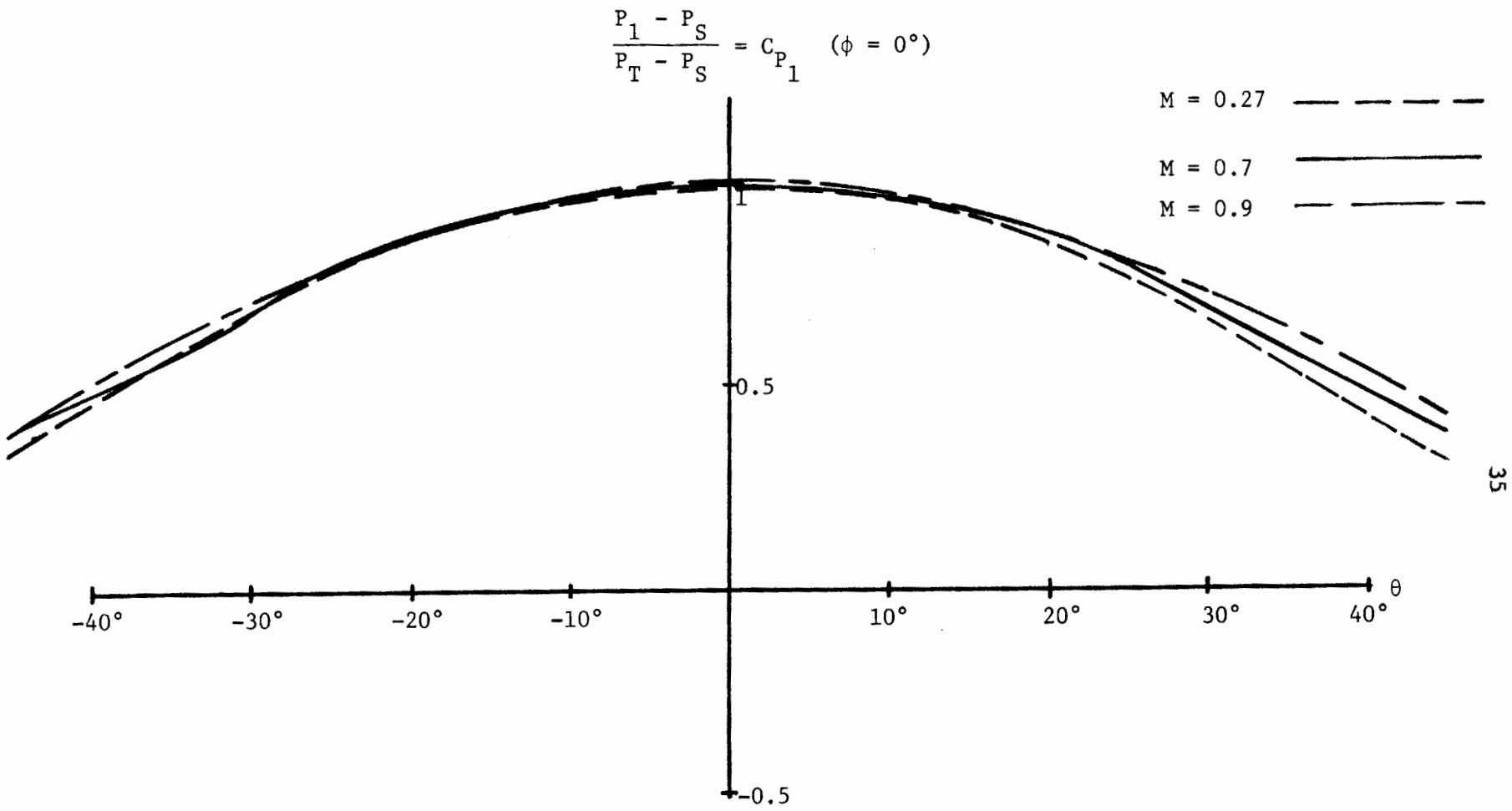

FIG. 23 - MACH NUMBER DEPENDENCE - P_1

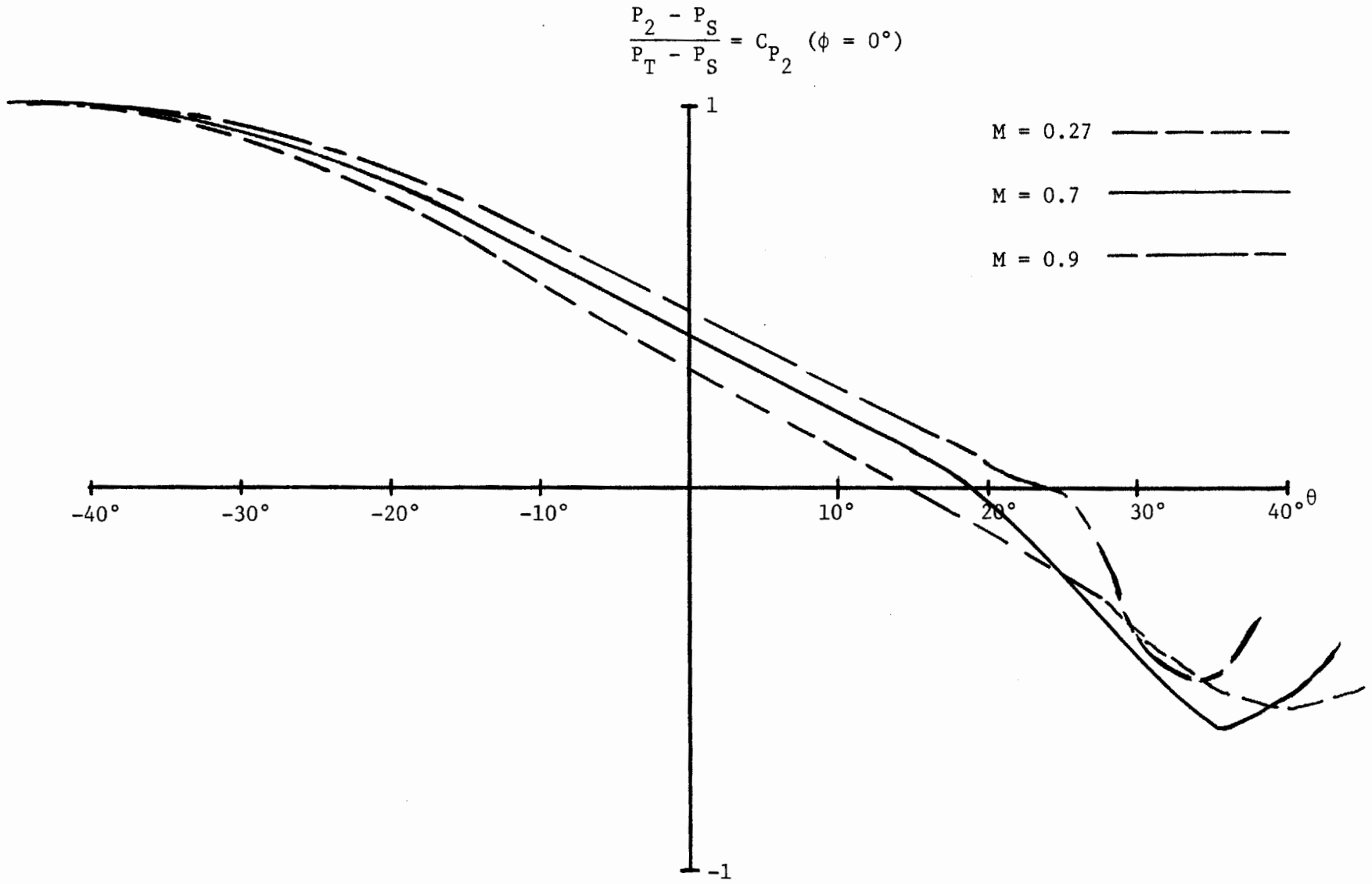

FIG. 24 - MACH NUMBER DEPENDENCE P_2

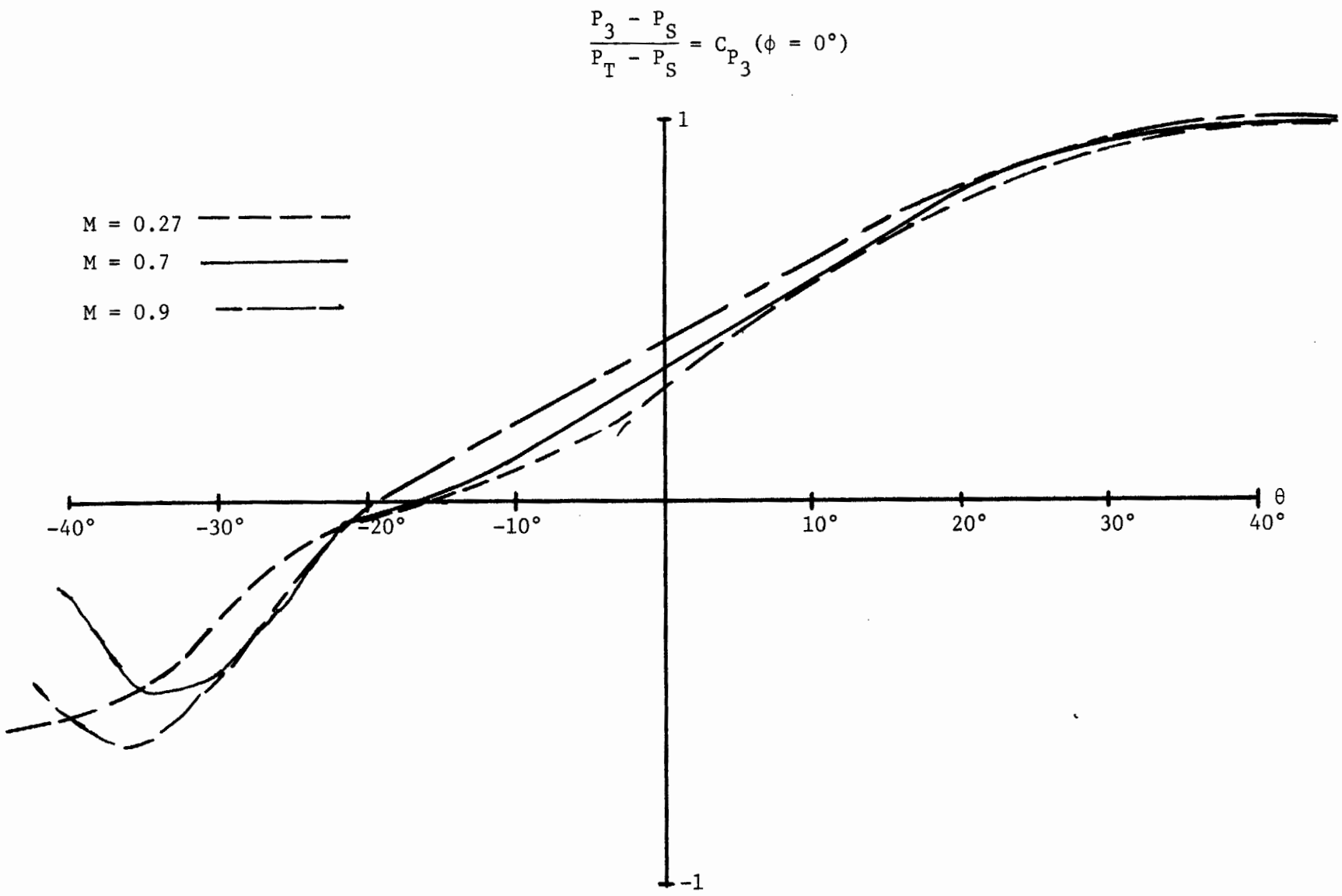

FIG. 25 - MACH NUMBER DEPENDENCE - P_3

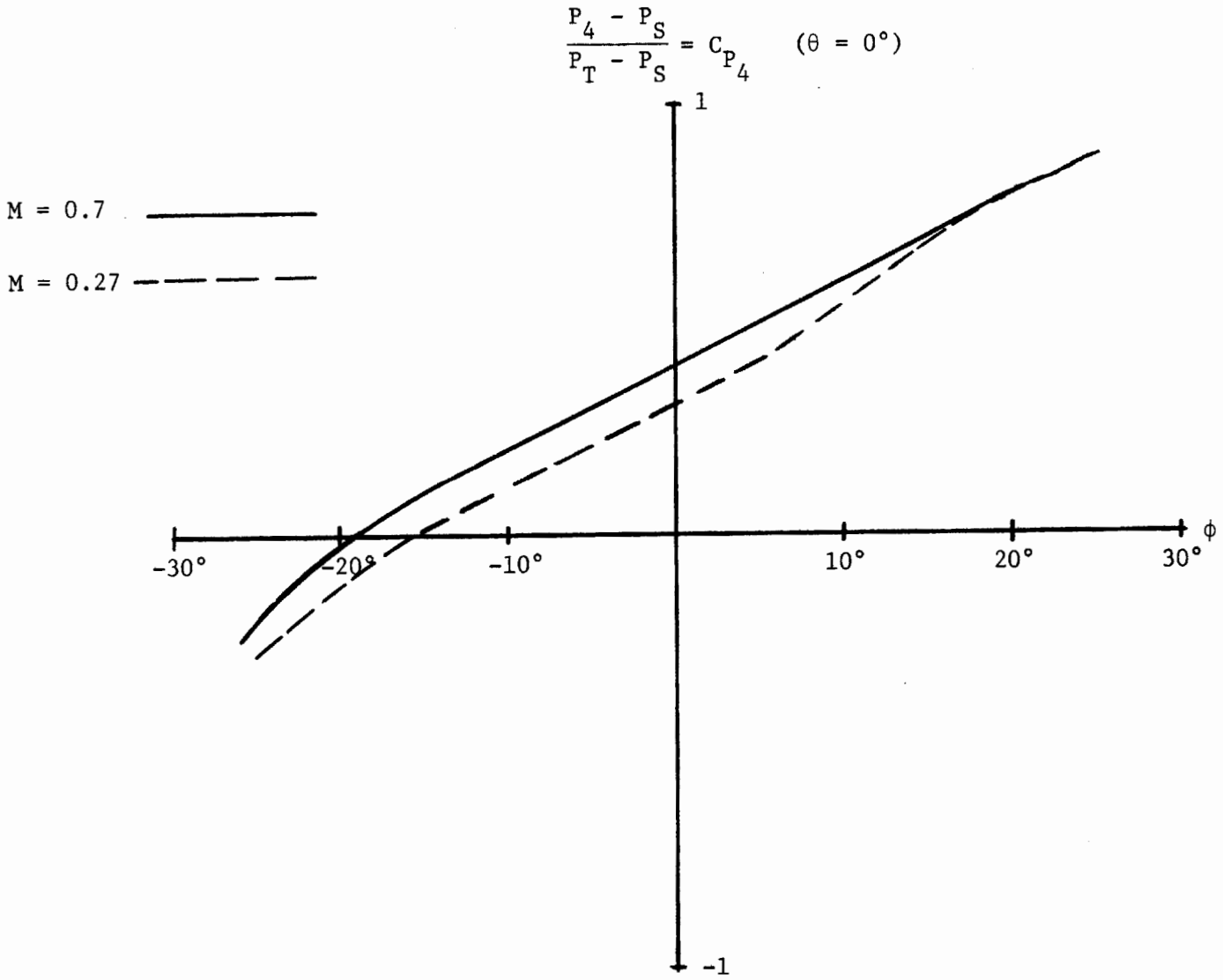

FIG. 26 - MACH NUMBER DEPENDENCE - P_4

$$\frac{P_5 - P_S}{P_T - P_S} = C_{P_5} \quad (\theta = 0°)$$

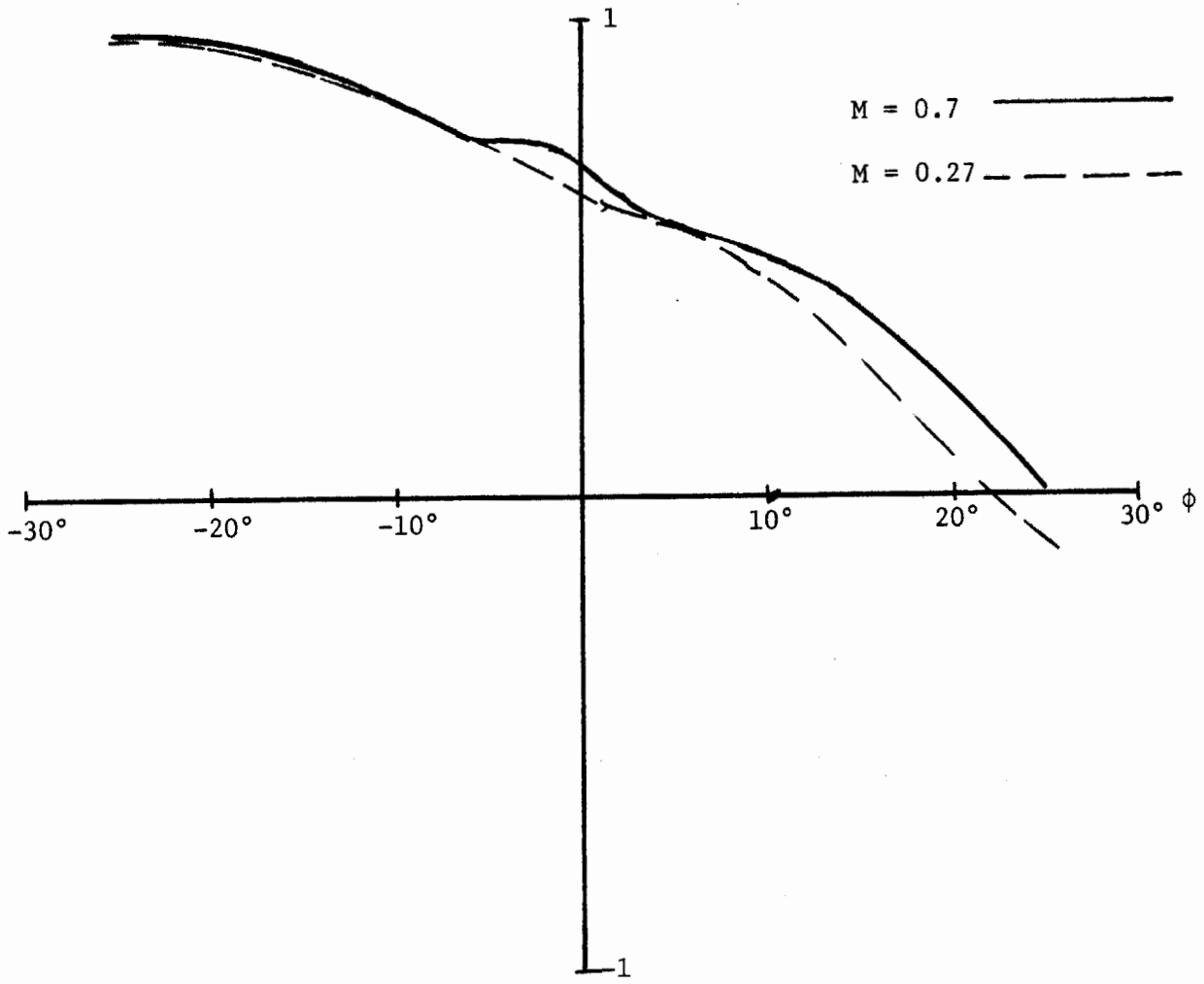

FIG. 27 - MACH NUMBER DEPENDENCE - P_5

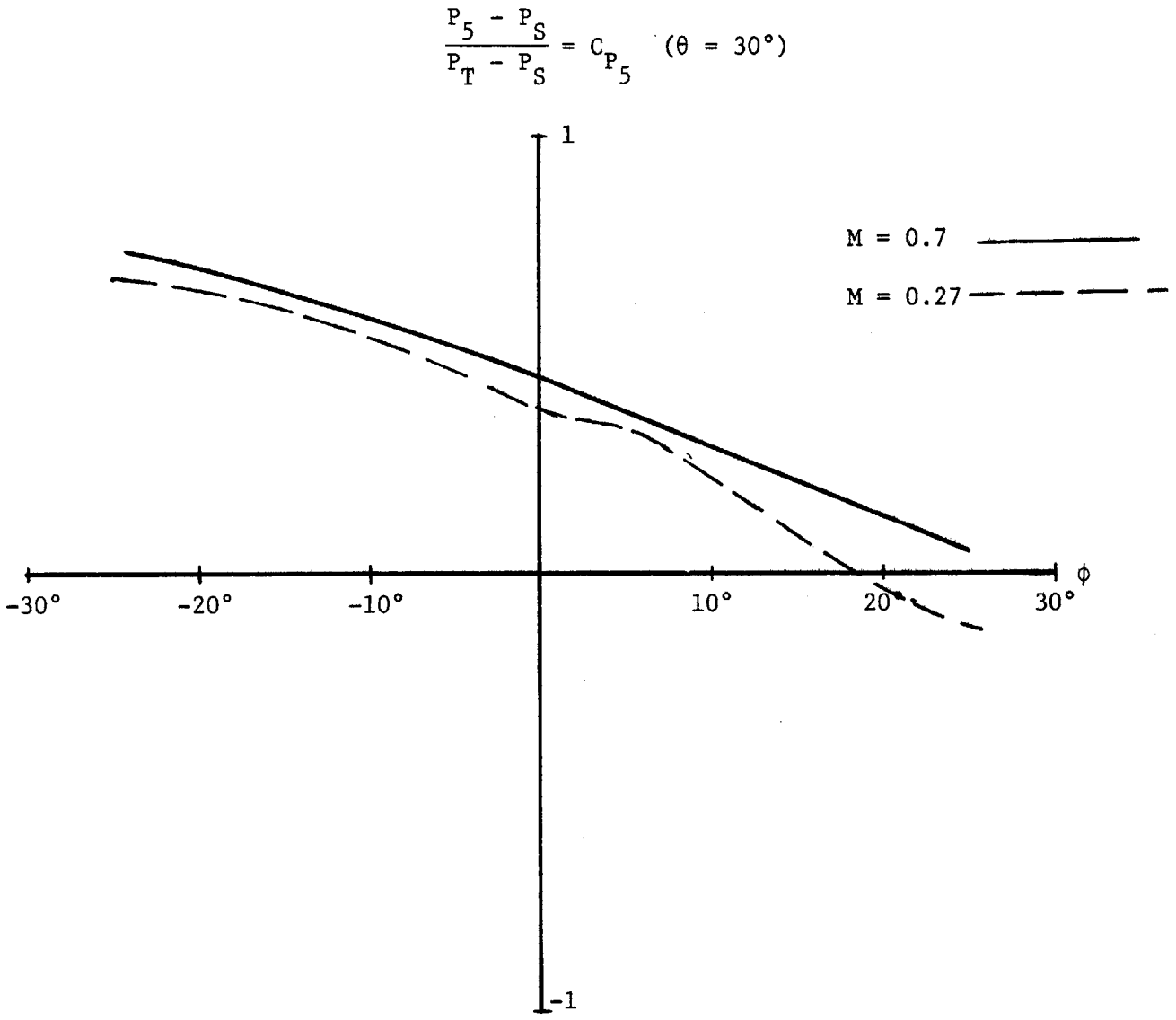

FIG. 28 - MACH NUMBER DEPENDENCE - P_5 AT θ = 30°

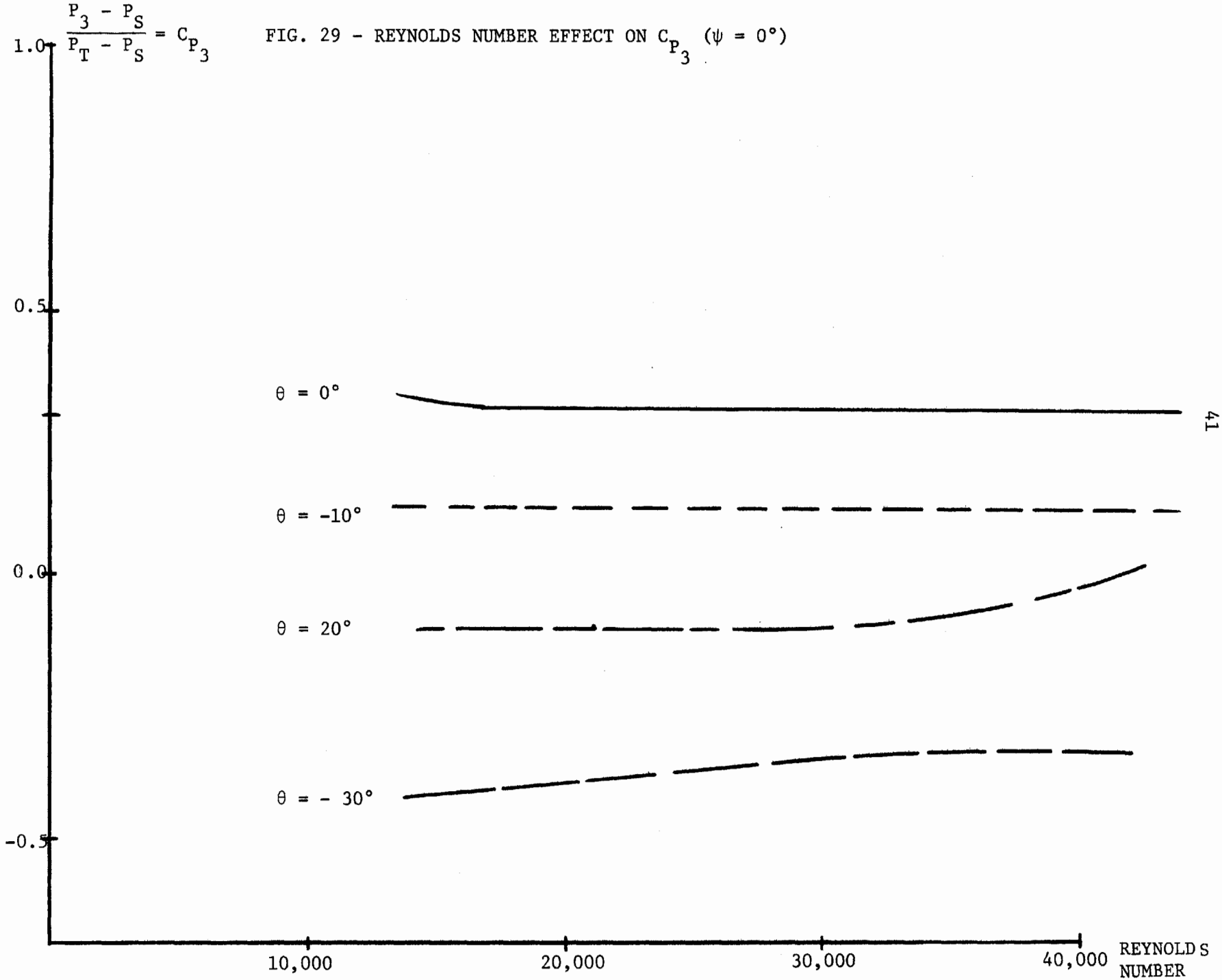

FIG. 29 - REYNOLDS NUMBER EFFECT ON C_{P_3} ($\psi = 0°$)

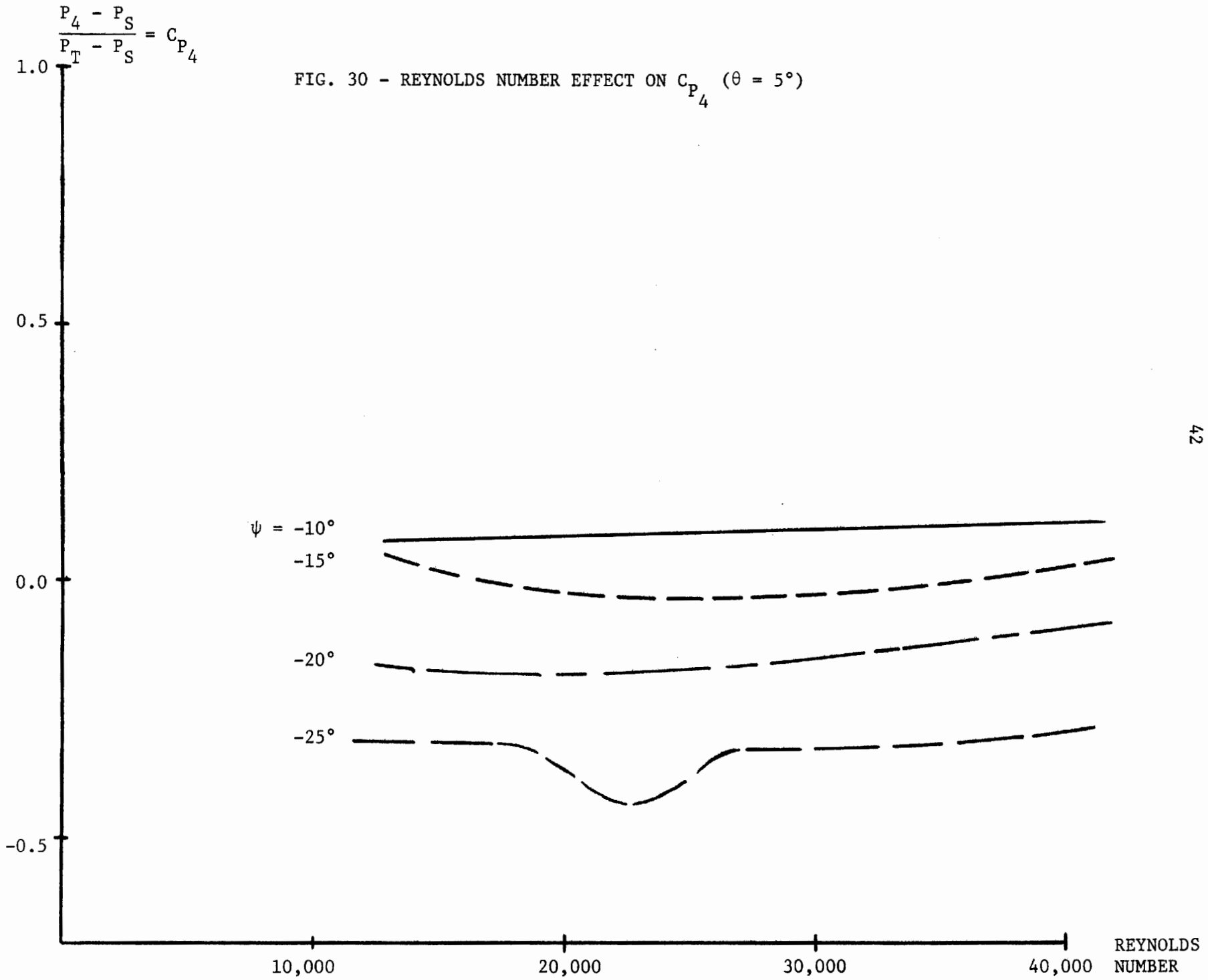

FIG. 30 - REYNOLDS NUMBER EFFECT ON C_{P_4} ($\theta = 5°$)

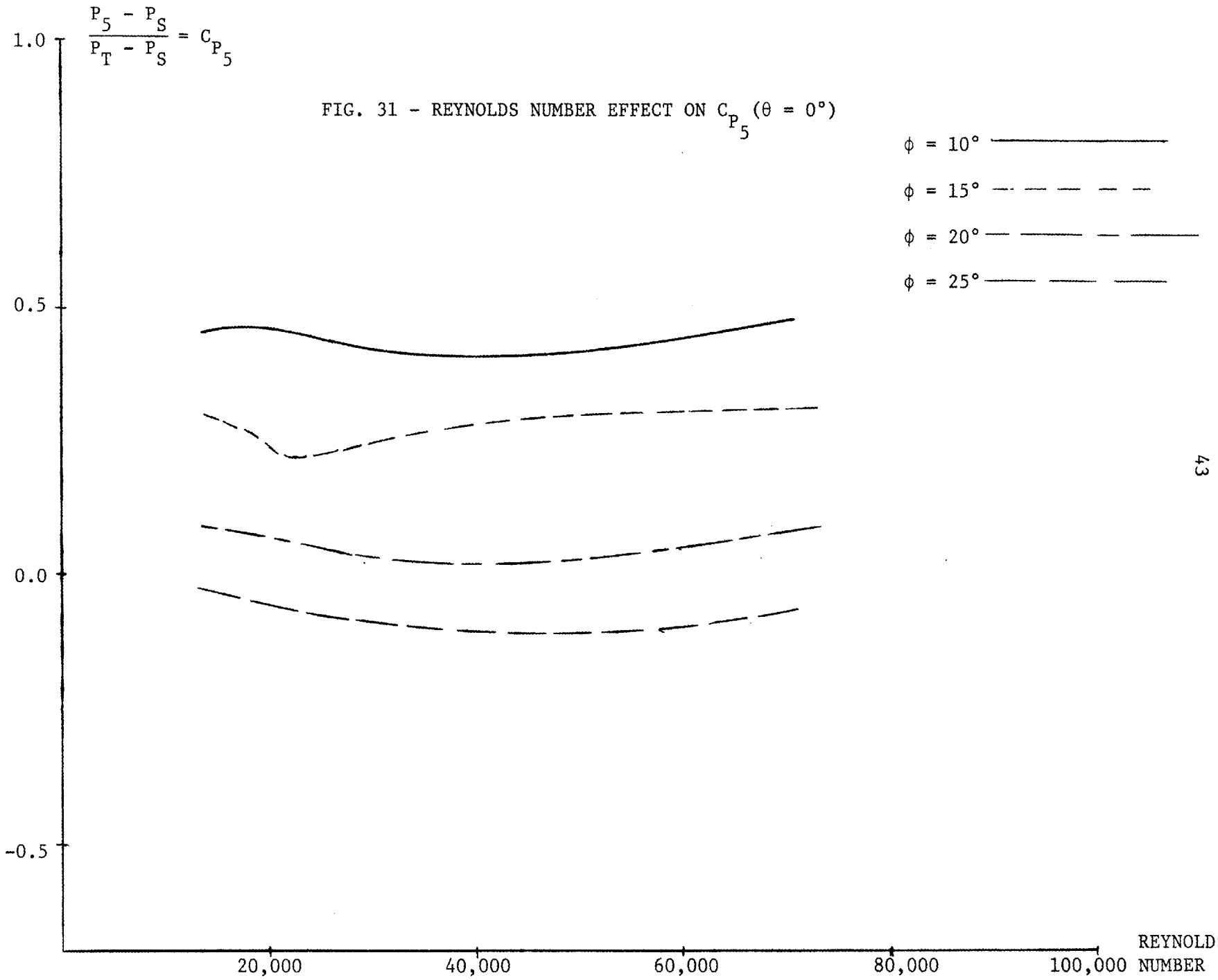

FIG. 31 - REYNOLDS NUMBER EFFECT ON C_{P_5} (θ = 0°)

APPENDIX

Theta Directional Calibration Points - F(θ, Mach Number)

	F(θ,0.27)			F(θ,0.7)		
θ	ϕ=-20°	ϕ=0°	ϕ=20°	ϕ=-25°	ϕ=0°	ϕ=25°
-40	-3.660	-3.27	-2.985	-4.889	-4.600	-2.166
-35	-2.493	-2.33	-2.675	-3.227	-2.00	-1.894
-30	-1.972	-1.698	-1.822	-1.724	-1.637	-1.674
-25	-1.453	-1.297	-1.324	-1.313	-1.245	-1.302
-20	-0.980	-0.853	-0.933	-0.937	-0.900	-0.950
-15	-0.639	-0.569	-0.664	-0.622	-0.648	-0.661
-10	-0.393	-0.347	-0.423	-0.427	-0.399	-0.413
- 5	-0.209	-0.176	-0.203	-0.216	-0.271	-0.221
0	-0.029	0.0	-0.035	-0.014	-0.014	-0.016
5	0.133	0.169	0.199	0.172	0.151	0.177
10	0.295	0.380	0.410	0.373	0.357	0.392
15	0.512	0.589	0.647	0.571	0.585	0.625
20	0.802	0.882	0.924	0.847	0.870	0.900
25	1.158	1.276	1.258	1.217	1.231	1.233
30	1.683	1.67	1.770	1.689	1.607	1.586
35	2.179	2.447	2.350	2.056	1.968	1.790
40	3.286	3.98	2.825	4.300	3.050	2.071

$F(\theta, 0.9)$

θ	$\phi=-25°$	$\phi=0°$	$\phi=25°$
-40	-5.158	-4.79	-2.71
-35	-2.349	-2.050	-1.755
-30	-1.595	-1.588	-1.456
-25	-1.177	-1.26	-1.225
-20	-0.950	-0.0651	-0.975
-15	-0.666	-0.6748	-0.707
-10	-0.432	-0.4356	-0.439
- 5	-0.226	-0.23	-0.222
0	0.0058	-0.005	-0.0057
5	0.211	0.1714	0.1785
10	0.474	0.3671	0.401
15	0.629	0.5840	0.631
20	0.884	0.8817	0.928
25	1.151	1.180	1.162
30	1.43	1.472	1.384
35	2.019	1.88	1.679
40	4.356	3.84	2.65

Phi Directional Calibration Points - F(ϕ,Mach Number)

F(ϕ,0.7)

ϕ	θ=-30°	θ=-20°	θ=0°	θ=20°	θ=30°
-25	2.33	2.039	1.803	1.836	2.101
-20	1.661	1.493	1.39	1.558	1.676
-15	1.203	1.104	1.044	1.114	1.26
-10	0.888	0.831	0.769	0.849	0.948
- 5	0.558	0.537	0.500	0.534	0.571
0	0.300	0.288	0.38	0.319	0.358
5	0.013	0.070	0.095	0.089	0.089
10	-0.233	-0.209	-0.116	-0.166	-0.147
15	-0.709	-0.603	-0.452	-0.519	-0.508
20	-1.25	-1.00	-0.849	-0.890	-0.979
25	-2.69	-2.167	-1.42	-1.68	-1.85

F(,0.27)

ϕ	θ=-30°	θ=-20°	θ=0°	θ=20°	θ=30°
-25	2.219	1.903	1.694	1.821	2.193
-20	1.586	1.457	1.343	1.426	1.573
-15	1.208	1.112	1.038	1.11	1.189
-10	0.778	0.729	0.722	0.739	0.771
- 5	0.566	0.523	0.516	0.522	0.549
- 0	0.314	0.311	0.336	0.295	0.271
5	0.103	0.155	0.181	0.127	0.119
10	-0.214	-0.124	-0.078	-0.136	-0.193
15	-0.634	-0.496	-0.447	-0.469	-0.561
20	-1.178	-0.986	-0.879	-0.908	-1.029
25	-2.503	-2.070	-1.419	-1.734	-1.889

Dynamic Head Calibration Points - H(θ, ϕ, Mach Number)

	H(θ,ϕ,0.27)			H(θ,ϕ,0.7)		
θ	ϕ=-20°	ϕ=0°	ϕ=+20°	ϕ=-25°	ϕ=0°	ϕ=+25°
-35	-1.746	-1.597	-2.012	-1.758	-1.245	-1.302
-30	-1.669	-1.337	-1.489	-1.429	-1.164	-1.36
-25	-1.243	-1.234	-1.234	-1.456	-1.104	-1.302
-20	-1.215	-1.055	-1.033	-1.22	-1.068	-1.153
-15	-1.039	-0.870	-0.924	-1.083	-0.940	-1.040
-10	-0.933	-0.782	-0.852	-1.013	-0.822	-0.955
- 5	-0.885	-0.712	-0.810	-0.959	-0.799	-0.932
0	-0.863	-0.713	-0.774	-0.937	-0.799	-0.917
5	-0.864	-0.757	-0.801	-0.955	-0.805	-0.935
10	-0.876	-0.803	-0.841	-0.996	-0.839	-0.975
15	-0.949	-0.880	-0.908	-1.054	-0.955	-1.031
20	-1.090	-0.958	-1.036	-1.204	-1.093	-1.149
25	-1.274	-1.163	-1.179	-1.416	-1.13	-1.289
30	-1.479	-1.302	-1.420	-1.588	-1.164	-1.282
35	-1.603	-1.631	-1.558	-1.618	-1.237	-1.155

$H(\theta,\phi,0.9)$

θ	$\phi=-25°$	$\phi=0°$	$\phi=+25°$
-35	-2.215	-1.37	-1.26
-30	-1.454	-1.121	-1.118
-25	-1.055	-1.094	-1.12
-20	-1.18	-1.11	-1.193
-15	-1.098	-1.038	-1.15
-10	-1.038	-0.948	-1.10
- 5	-1.022	-0.899	-1.080
0	-0.977	-0.910	-1.080
5	-1.003	-0.915	-1.06
10	-1.151	-0.925	-1.084
15	-1.070	-1.018	-1.12
20	-1.33	-1.13	-1.22
25	-1.027	-1.11	-1.096
30	-1.203	-1.073	-1.05
35	-1.79	-1.26	-1.182

Static Pressure Calibration Points - $K_{P_N}(\theta,\phi,\text{Mach Number})$

	$K_{P_1}(\theta,\phi,0.7)$			$K_{P_2}(\theta,\phi,0.7)$		
θ	ϕ=−25°	ϕ=0°	ϕ=+25°	ϕ=−25°	ϕ=0°	ϕ=+25°
−35	−0.636	−0.718	−0.497	−1.259	−1.218	−0.944
−30	−0.607	−0.781	−0.622	−0.969	−1.100	−0.959
−25	−0.750	−0.854	−0.709	−0.906	−0.976	−0.855
−20	−0.707	−0.909	−0.703	−0.675	−0.859	−0.678
−15	−0.691	−0.856	−0.969	−0.502	−0.680	−0.527
−10	−0.698	−0.797	−0.690	−0.409	−0.497	−0.397
− 5	−0.686	−0.786	−0.695	−0.294	−0.391	−0.305
0	−0.688	−0.799	−0.702	−0.195	−0.306	−0.210
5	−0.693	−0.801	−0.710	−0.107	−0.226	−0.121
10	−0.695	−0.821	−0.713	−0.004	−0.143	−0.017
15	−0.683	−0.886	−0.719	0.103	−0.093	0.094
20	−0.709	−0.949	−0.736	0.214	−0.014	0.214
25	−0.735	−0.889	−0.739	0.373	0.226	0.378
30	−0.689	−0.811	−0.635	0.655	0.493	0.657
35	−0.583	−0.732	−0.480	0.944	0.753	0.915

	$K_{P_3}(\theta,\phi,0.7)$			$K_{P_2}(\theta,\phi,0.27)$		
θ	$\phi=-25°$	$\phi=0°$	$\phi=+25°$	$\phi=-20°$	$\phi=0°$	$\phi=+20°$
-35	0.977	0.782	0.950	-1.384	-1.569	-1.650
-30	0.755	0.537	0.715	-1.262	-1.250	-1.166
-25	0.406	0.269	0.447	-1.075	-1.070	-0.898
-20	0.262	0.041	0.272	-0.770	-0.821	-0.671
-15	0.120	-0.32	0.134	-0.562	-0.582	-0.517
-10	0.013	-0.048	0.017	-0.411	-0.432	-0.388
- 5	0.079	-0.180	-0.084	-0.311	-0.297	-0.271
0	-0.181	-0.293	-0.194	-0.216	-0.212	-0.168
5	-0.279	-0.377	-0.298	-0.129	-0.166	-0.075
10	-0.381	-0.500	-0.402	-0.040	-0.085	-0.024
15	-0.469	-0.679	-0.531	0.051	0.004	0.129
20	-0.633	-0.884	-0.687	0.162	0.122	0.233
25	-0.843	-1.005	-0.856	0.321	0.245	0.385
30	-1.034	-1.114	-0.928	0.610	0.492	0.632
35	-1.111	-1.216	-0.875	0.960	0.851	1.447

$K_{P_2}(\theta,\phi,0.9)$

θ	ϕ=-25°	ϕ=0°	ϕ=+25°
-35	-1.651	-1.349	-0.924
-30	-1.038	-1.062	-0.793
-25	-0.706	-0.989	-0.749
-20	-0.724	-0.933	-0.737
-15	-0.591	-0.786	-0.625
-10	-0.470	-0.631	-0.509
- 5	-0.376	-0.509	-0.411
0	-0.244	-0.412	-0.320
5	-0.150	-0.324	-0.215
10	-0.045	-0.222	-0.101
15	0.070	-0.163	0.018
20	0.231	-0.059	0.157
25	0.481	0.183	0.420
30	0.589	0.455	0.627
35	0.717	0.638	0.789

REFERENCES

1. Dean,Jr., R. C., "Aerodynamic Measurements," MIT Gas Turbine Lab. Report No. 22-N, 1953.

2. Duncan, Thom, and Young, Mechanics of Fluids, American Elsevier Publishing Company, Inc., 1970, pp. 252-254, 365-367.

3. Gorlin, S. M., and Slezinger, I. I., "Wind Tunnels and Their Instrumentations," NASA TT F-346, 1966, pp. 173-175, 201-204.

4. Kerrebrock, J. L., "The MIT Blowdown Compressor Facility," MIT Gas Turbine Lab. Report No. 108, 1972, pp. 13-16.

5. Liepman, H. W., and Puckett, A. E., Introduction to Aerodynamics of a Compressible Fluid, John Wiley and Sons, Inc., 1947, pp. 26-30.

6. Pankhurst, R. C., and Bryer, D. W., Pressure-Probe Methods for Determining Wind Speed and Flow Direction, Her Majesty's Stationary Office, London, 1971, pp. 67-74.

7. Schlichting, H., Boundary-Layer Theory, McGraw-Hill Book Company, 1968, pp. 590-609.

8. Shapiro, H. A., The Dynamics and Thermodynamics of Compressible Fluid Flow, Vol. 1, The Ronald Press Company, New York, 1953, p. 368.

9. Thompkins, W. T., "An Experimental and Computational Study of the Flow in a Transonic Compressor Rotor," MIT Gas Turbine Lab. Report No. 129, 1976, pp. 18-21.